Dielectronic recombination of Er-like tungsten

U. I. Safronova and A. S. Safronova

Physics Department, University of Nevada, Reno, Nevada 89557, USA
(Received 21 January 2012; published 5 March 2012)

Theoretical studies of dielectronic recombination, a very important process for both atomic and plasma physics, are carried out for low-ionized Er-like W. The dielectronic recombination (DR) of the Er-like ion W^{6+} proceeds via electron capture into the intermediate autoionizing states of the Tm-like ion W^{5+} followed by the radiative decay to singly-excited bound states. In particular, energy levels, radiative transition probabilities, and autoionization rates for $[Cd]4f^{14}5p^55l'nl$, $[Cd]4f^{14}5p^56l''nl$, $[Cd]4f^{13}5p^65l'nl$, and $[Cd]4f^{13}5p^66l''nl$ ($l' = d,f,g$, $l'' = s,p,d,f,g$, $n = 5$–7) states in Tm-like tungsten (W^{5+}) are calculated using the relativistic many-body perturbation theory and relativistic all-order single-double method as well as the Hartree-Fock-relativistic method (COWAN code). Branching ratios relative to the first threshold and intensity factors are calculated for satellite lines. DR rate coefficients are determined for the singly-excited $[Cd]4f^{14}5p^6nl$ ($n = 5$–7) and nonautoionizing doubly-excited $[Cd]4f^{14}5p^55d^2$, $[Cd]4f^{13}5p^65d^2$, $[Cd]4f^{13}5p^66s^2$, $[Cd]4f^{13}5p^65d6s$, and $[Cd]4f^{13}5p^65d6p$ states. Also, contributions from the autoionizing doubly-excited $[Cd]4f^{14}5p^55l'nl$, $[Cd]4f^{14}5p^56l''nl$, $[Cd]4f^{13}5p^65l'nl$, and $[Cd]4f^{13}5p^66l''nl$ states (with n up to 100), which are very important for calculating total DR rates, are estimated. Synthetic dielectronic satellite spectra from Tm-like W are simulated in a broad spectral range from 140 to 1200 Å. These relativistic calculations provide recommended values critically evaluated for their accuracy for a number of W^{5+} ion properties useful for a variety of applications, including for fusion applications.

I. INTRODUCTION

Dielectronic recombination (DR) process in tungsten ions was investigated recently in a number of publications [1–10]. Excitation energies, radiative and autoionization rates, dielectronic satellite lines, and dielectronic recombination rates for excited states of Ag-like W^{27+} from Pd-like W^{28+} were given in Ref. [2]. Dielectronic satellite lines and dielectronic recombination rates for excited states of Na-like W from Ne-like W and for excited states of Mg-like W from Na-like W were presented by Safronova *et al.* in Refs. [5,6], respectively. The relativistic many-body perturbation theory method (RMBPT code), the multiconfiguration relativistic Hebrew University Lawrence Atomic Code (HULLAC code), and the Hartree-Fock-relativistic (HFR) method (COWAN code) were used to perform a large-scale calculation of atomic parameters (excitation energies, radiative, and autoionization rates) to evaluate dielectronic recombination rate coefficients and build synthetic satellite spectra.

Dielectronic recombination of xenon-like W^{20+} forming W^{19+} was studied recently [1] experimentally at a heavy-ion storage ring. A merged-beams method was employed for obtaining absolute rate coefficients for electron-ion recombination in the collision-energy range of 0–140 eV. X-ray spectroscopic measurements of the dielectronic recombination LMn ($n = 3$–10) resonances of W^{60+} to W^{67+} ions were performed by Biedermann and Radtke in Ref. [7]. Dielectronic and radiative recombination of Si- to N-like tungsten ions was investigated by Biedermann *et al.* in Ref. [8]. Highly charged Si-like W^{60+} to N-like W^{67+} ions were produced, stored, and excited using the Berlin EBIT. The measurement of x rays from $n = 2$–3, 2–4, and higher DR resonance transitions was compared to relativistic calculations of the DR cross sections and rate coefficients carried out with the HULLAC code [8].

Dielectronic recombination of yttrium-like W^{35+} was recently studied theoretically [11] using the configuration-average distorted-wave (CADW) method. Authors presented results for CADW rate coefficients for both $\Delta n = 0$ and $\Delta n = 1$ excitations for this ion. It was underlined that they completed term-resolved and level-resolved semirelativistic distorted-wave and level-resolved relativistic R-matrix DR calculations for the $4d \rightarrow 4f$ and $4p \rightarrow 4d$ excitations from the levels of the $4s^24p^64d^3$ ground configuration of W^{35+} and compared the cross sections and rate coefficients with those calculated using a semirelativistic CADW method. *Ab initio* calculation of the total dielectronic recombination (DR) rate coefficients from the ground state $3s^23p^63d^9$ of Co-like tungsten was performed using the flexible atomic code (FAC) [9,10]. The results show that the complex series $3p^63d^84ln'l'$ give the most important contribution (>66%) to the total DR rate coefficient. The complex $3p^53d^{10}n'l'$, $3p^53d^94ln'l'$, and $3p^63d^85ln'l'$ series can also give significant contributions to the total DR rates at relatively high electron temperature [10].

Dalhed *et al.* [12] underlined that their paper presented the first explicit calculation of the partial dielectronic-recombination-rate coefficients via $3l3l'$ manifold for 17 Ne-like ions ranging from Ar^{8+} to W^{64+}, using relativistic multconfiguration wave functions to calculate both the Auger and radiative matrix elements. Unfortunately, no numerical results were given for those atomic properties. Several years later, dielectronic recombination of Ni-, Cu-, and Ar-like tungsten through low inner-shell excited configuration including collision processes was considered in Ref. [13]. A general analytic formula for total dielectronic recombination rate coefficients of Ni-like ions was given in Ref. [14]. Relativistic calculations of the dielectronic recombination cross sections and rate coefficient for Ne-like tungsten (W^{64+}) in the $2s^22p^6$ ground state were performed by Behar *et al.* [15,16]. The DR contributions of the most important Na-like doubly-excited configuration complexes, namely, $(2s2p)^73ln'l'$ ($n = 3$–13) and $(2s2p)^74l4l'$ were calculated by level-by-level

computations. All of the basic atomic quantities used in those calculations were obtained using HULLAC code. The HULLAC code was also used by Peleg *et al.* in Ref. [17] to evaluate the total dielectronic recombination rate coefficient for Ar-like tungsten, W^{56+}. *Ab initio* calculations of the total dielectronic recombination rate coefficient of Ni-like tungsten (W^{46+}) in the ground state were performed by Behar *et al.* [18] using the HULLAC atomic code package. Their level-by-level calculations include the DR contributions of all of the levels (over 17000) in the Cu-like inner-shell excited configurations $3d^9 4lnl'$ ($n' \leqslant 9$), $3p^5 3d^{10} 4lnl'$ ($n' \leqslant 5$), and $3s3p^6 3d^{10} 4lnl'$ ($n' \leqslant 5$) [18].

In the present work, we evaluate the total DR rate coefficient of Er-like tungsten (W^{6+}) and DR rate coefficients for the first excited odd- and even-parity states in Tm-like tungsten (W^{5+}). The present level-by-level calculations include the DR contributions of all of the levels (over 16000) in the Tm-like inner-shell excited configurations $[Cd]4f^{14}5p^5 5l'nl$, $[Cd]4f^{14}5p^5 6l''nl$, $[Cd]4f^{13}5p^6 5l'nl$, and $[Cd]4f^{13}5p^6 6l''nl$ ($l' = d,f$, $l'' = s,p,d,f$, and $n = 5$–7).

Energy levels, radiative transition probabilities, and autoionization rates for those states are calculated using the Hartree-Fock-relativistic method (COWAN code) and the relativistic many-body perturbation theory method (RMBPT code). These two codes allow us to check the accuracy of our calculations and to achieve confidence that our predictions are reliable. It should be noted that there are only 14 available values for energies of W^{5+} presented in a NIST publication [19] for comparison. Then, in addition, we present a detailed comparison of our theoretical calculations with the recommended data from the NIST database to test the accuracy of our results. The state-selective DR rate coefficients to excited states of Tm-like tungsten, as well as the total DR rate coefficients as a function of electron temperature, are evaluated. The present paper continues our efforts on the calculation of the DR rate coefficients that were previously determined for C I [20], C II [21,22], C III [23], O IV [24], O V [25], Ne VII [26], Ne VI [27], Mg-like Fe [28], Mg-like Zn, Kr, and Mo [29], K-like Ni [30], Ag-like Xe [31], and high-ionization stages of W, such as Li-like tungsten [4], Na-like tungsten [5], and Mg-like tungsten [6].

II. ENERGY LEVELS, TRANSITION PROBABILITIES, AND AUTOIONIZATION RATES IN Tm-LIKE TUNGSTEN

We carried out detailed calculations of the radiative and autoionization rates for the $4f^{14}5p^5 5l'nl$, $4f^{14}5p^5 6l''nl$, $4f^{13}5p^6 5l'nl$, and $4f^{13}5p^6 6l''nl$ ($l' = d,f,g$, $l'' = s,p,d,f,g$, and $n = 5$–7) intermediate states in Tm-like tungsten (W^{5+}). We omit the core $[Cd] = 1s^2 2s^2 2p^6 3s^2 3p^6 3d^{10} 4s^2 4p^6 4d^{10} 5s^2$ here and in text below from the configuration notation. The list of the $4f^{14}5p^6 nl$, $4f^{14}5p^5 5l'nl$, $4f^{14}5p^5 6l''nl$, $4f^{13}5p^6 5l'nl$, and $4f^{13}5p^6 6l''nl$ ($l' = d,f,g$, $l'' = s,p,d,f,g$, and $n = 5$–7) configurations is given in Table I. There are 78 even-parity and 82 odd-parity configurations. There are 14 even-parity levels and 10 odd-parity levels of the singly-excited $4f^{14}5p^6 nl$ configurations with $n = 5$–7. The set of doubly-excited $4f^{14}5p^5 5l'nl$ and $4f^{14}5p^5 6l'nl$ configurations with $n = 5$–7

consists of 3140 even-parity and 2990 odd-parity levels, while the set of $4f^{13}5p^6 5l'nl$ and $4f^{13}5p^6 6l'nl$ configurations from Table I contains 5280 even-parity and 4900 odd-parity levels.

The atomic energy levels, radiative transition probabilities, and autoionization rates were obtained by using the atomic structure COWAN code [32]. The scaling of electrostatic integrals in COWAN code allows one to correct for correlation effects and obtain good agreement with experimental energies. We used the same scaling factor (0.85) for all electrostatic integrals. We used a modified version of COWAN code freely distributed by Dr. A. Kramida via the Internet [33]. That version of computer code allows one to remove transitions with small values of transition rates $A_r, A_r < 10^5 \text{ s}^{-1}$. Even with this restriction, the resulting list of radiative transitions between the $4f^{14}5p^6 nl$, $4f^{14}5p^5 5l'nl$, $4f^{14}5p^5 6l''nl$, $4f^{13}5p^6 5l'nl$, and $4f^{13}5p^6 6l''nl$ ($l' = d,f,g, l'' = s,p,d,f,g$, and $n = 5$–7) states consists of 1.5×10^6 transitions.

In order to check the accuracy of those calculations, we carried out additional calculations using the second-, third-, and all-order relativistic perturbation theory. We carry out the RMBPT calculations using two methods, second- and third-order RMBPT, described in [34], and the relativistic all-order single-double (SD) method, described in [35,36] and references therein. The SD method includes correlation corrections in a more complete way and is expected to yield more accurate results, especially when correlation corrections are significant. While the SD method includes fourth- and higher-order terms, it omits some third-order terms. These omitted terms are identified and added to our SD data (see [36] for details).

We use the *B*-spline method [37] to generate a complete set of basis Dirac-Fock (DF) orbitals for use in the evaluation of RMBPT expressions. For Tm-like W^{5+}, we use 50 splines of order $k = 9$ for each angular momentum. The basis orbitals are constrained to a spherical cavity of radius $R = 30$ a.u. The cavity radius is chosen large enough to accommodate all nl_j orbitals considered here and small enough that 50 splines can approximate inner-shell DF wave functions with good precision. We use 40 out of 50 basis orbitals for each partial wave in our third-order and all-order energy calculations, since contributions from higher-energy orbitals are negligible.

Results of our energy calculations for the 21 $4f^{14}5p^6 nl$ levels of W^{5+} are summarized in Table II. Columns 3–6 of Table II give the lowest-order DF energies $E^{(\text{DF})}$ and the second- and third-order Coulomb correlation energies, $E^{(\text{DF}+2)}$ and $E^{(\text{DF}+2+3)}$. We list the all-order SD energies in the column labeled $E^{(\text{DF}+\text{SD})}$. The COWAN code results are listed in column labeled $E^{(\text{COWAN})}$. The recommended NIST energies [19] are given in column labeled $E^{(\text{NIST})}$. The experimental data are not available for all levels. The largest disagreement (0.2%) between our $E^{(\text{DF}+\text{SD})}$ and $E^{(\text{NIST})}$ values is for the $5f\ ^2F_J$ levels. We also have an excellent agreement (0.01% or 36 cm^{-1}) between our $E^{(\text{DF}+\text{SD})}$ and $E^{(\text{NIST})}$ values for ionization potential (last line of Table II). The NIST value has 0.06% uncertainty (522370 ± 300) [19]. The energies given in the column labeled $E^{(\text{COWAN})}$ are in a good agreement with energies given in the column labeled $E^{(\text{DF}+2)}$. This signifies that the large portion of correlation contribution is taken into account by the COWAN code [32].

TABLE I. List for 78 even-parity and 82 odd-parity configurations in Tm-like W^{5+}; designations: $4f^{14}5p^6nl = nl$, $4f^{14}5p^5nln'l' = 5pnln'l'$, and $4f^{13}5p^6nln'l' = 4fnln'l'$.
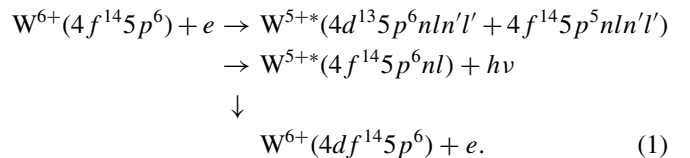
	Even-parity states						Odd-parity states				
N	Conf.	N	Conf.	N	Conf.	N	Conf.	N	Conf.	N	Conf.
1	$5d$	28	$4f5d7p$	55	$5p6f7d$	1	$5f$	28	$4f5f^2$	55	$5p6d7g$
2	$5g$	29	$4f5d7f$	56	$5p6f7g$	2	$6p$	29	$4f5g^2$	56	$5p6p7f$
3	$6s$	30	$4f5f5g$	57	$5p6g6p$	3	$6f$	30	$4f6s^2$	57	$5p6p7f$
4	$6d$	31	$4f5f6s$	58	$5p6g6f$	4	$7p$	31	$4f5d5g$	58	$5p6f7p$
5	$6g$	32	$4f5f6d$	59	$5p6g7p$	5	$7f$	32	$4f5d6s$	59	$5p6f7p$
6	$7s$	33	$4f5f6g$	60	$5p6g7f$	6	$5p5d^2$	33	$4f5d6d$	60	$5p6g6s$
7	$7d$	34	$4f5f7s$	61	$4f6s6p$	7	$5p5f^2$	34	$4f5d6g$	61	$5p6g6d$
8	$7g$	35	$4f5f7d$	62	$4f6s6f$	8	$5p5g^2$	35	$4f5d7s$	62	$5p6g7s$
9	$5p5d5f$	36	$4f5f6p$	63	$4f6s7p$	9	$5p6s^2$	36	$4f5d7d$	63	$5p6g7d$
10	$5p5d6p$	37	$4f5f6f$	64	$4f6s7f$	10	$5p5d5g$	37	$4f5f6p$	64	$5p6g7g$
11	$5p5d6f$	38	$4f5f7p$	65	$4f6d6p$	11	$5p5d6s$	38	$4f5f6f$	65	$4f6d^2$
12	$5p5d7p$	39	$4f5d6p$	66	$4f6d6f$	12	$5p5d6d$	39	$4f5f7p$	66	$4f6f^2$
13	$5p5d7f$	40	$5p6s6p$	67	$4f6d7p$	13	$5p5d6g$	40	$4f5f7f$	67	$4f6d6s$
14	$5p5f5g$	41	$5p6s6f$	68	$4f6d7f$	14	$5p5d7s$	41	$4f5g6s$	68	$4f6d6g$
15	$5p5f6s$	42	$5p6s7p$	69	$4f6p7s$	15	$5p5d7d$	42	$4f5g6d$	69	$4f6s7s$
16	$5p5f6d$	43	$5p6s7f$	70	$4f6p7d$	16	$5p5d7g$	43	$4f5g7s$	70	$4f6s7d$
17	$5p5f6g$	44	$5p6d6p$	71	$4f6p7g$	17	$5p5f6p$	44	$4f5g7d$	71	$4f6s7g$
18	$5p5f7s$	45	$5p6d6f$	72	$4f6f6s$	18	$5p5f6f$	45	$5p6d^2$	72	$4f6d7s$
19	$5p5f7d$	46	$5p6d7p$	73	$4f6f6d$	19	$5p5f7p$	46	$5p6f^2$	73	$4f6d7d$
20	$5p5f7g$	47	$5p6d7f$	74	$4f6f7s$	20	$5p5f7f$	47	$5p6g^2$	74	$4f6d7g$
21	$5p5g6p$	48	$5p6p7s$	75	$4f6f7d$	21	$5p5g6s$	48	$5p6d6s$	75	$4f6p7f$
22	$5p5g6f$	49	$5p6p7d$	76	$4f6f7g$	22	$5p5g6d$	49	$5p6d6g$	76	$4f6p7f$
23	$5p5g7p$	50	$5p6p7g$	77	$4f6g6p$	23	$5p5g6g$	50	$5p6s7s$	77	$4f6f7p$
24	$5p5g7f$	51	$5p6f6s$	78	$4f6g6f$	24	$5p5g7s$	51	$5p6s7d$	78	$4f6f7p$
25	$4f5d5f$	52	$5p6f6d$			25	$5p5g7d$	52	$5p6s7g$	79	$4f6g6s$
26	$4f5d6p$	53	$5p6f6g$			26	$4f6s^2$	53	$5p6d7s$	80	$4f6g6d$
27	$4f5d6f$	54	$5p6f7s$			27	$4f5d^2$	54	$5p6d7d$	81	$4f6g7s$
										82	$4f6g7d$

In Table III, we present wavelengths (λ in Å), oscillator strengths (f), and transition rates (gA_r) for the $4f^{14}5p^6nl$ and $4f^{14}5p^6n'l'$ transitions of Tm-like tungsten. Oscillator strengths and transition rates are calculated to the first, second, third, and all orders of RMBPT as well as in HFR approximation (COWAN code). We list available NIST data [19] in the column labeled "Recom." We also use these data to evaluate gf oscillator strengths and gA_r transition rates. We did not find experimental energy values for some of the levels presented in Table III. We put our SD all-order values from Table II in such cases and labeled them with an asterisk in the column "Recom." of Table III. The difference in oscillator strengths and transition rates is about 20%–50% for the largest gf and gA_r values and a factor of 2–5 for the smallest ones. Such a large difference is due to a large contribution of correlation effects (compare values given in columns "DF" and "DF + 2" of Table III). The difference between gf and gA_r values given in columns "DF + 2," "DF + 2 + 3," and "DF + SD" is smaller (about 10–20%). The gf and gA_r values in the column labeled as "COWAN" are in better agreement with gf and gA_r values in column "DF + 2" than in column "DF." That confirms once more that the correlation effects are partially included in the COWAN code with scaling of electrostatic integrals. For the purpose of this comparison, the gf and gA_r values in the column "COWAN" are recalculated using the recommended values of energies instead of the ones obtained from the COWAN code.

III. DIELECTRONIC SATELLITE SPECTRA IN Tm-LIKE TUNGSTEN

The dielectronic recombination of the Er-like ion W^{6+} proceeds via electron capture into the intermediate autoionizing states of the Tm-like ion W^{5+} followed by the radiative decay to singly-excited bound states:

$$
\begin{aligned}
\mathrm{W}^{6+}(4f^{14}5p^6) + e &\rightarrow \mathrm{W}^{5+*}(4d^{13}5p^6nln'l' + 4f^{14}5p^5nln'l') \\
&\rightarrow \mathrm{W}^{5+*}(4f^{14}5p^6nl) + h\nu \\
&\downarrow \\
&\quad \mathrm{W}^{6+}(4df^{14}5p^6) + e.
\end{aligned}
\tag{1}
$$

An alternative decay channel for the autoionizing state in Eq. (1) is via autoionization. In this case, the system returns to its original state $4f^{14}5p^6$ as shown by a vertical arrow in Eq. (1).

Importantly, not all of the doubly-excited states listed in the previous section can autoionize. The $4f^{14}5p^55l'nl$ ($l' = f,g$), $4f^{14}5p^56l'nl$ ($l' = p,d,f,g$), $4f^{13}5p^65l'nl$ ($l' = f,g$), and $4f^{13}5p^66l''nl$ ($l' = p,d,f,g$) and $l = s,p,d,f,g$, $n = 6$–7 states are indeed autoionizing states. However, the doubly-

TABLE II. Energies (E in cm^{-1}) calculated to the first, second, third, and all orders of RMBPT for the $4f^{14}5p^6nl$ states of Tm-like W^{5+}. Comparison of the RMBPT and COWAN results with recommended NIST data [19]. See text for further explanations.

Level	$E^{\text{(COWAN)}}$	$E^{\text{(DF)}}$	$E^{\text{(DF+2)}}$	$E^{\text{(DF+2+3)}}$	$E^{\text{(DF+SD)}}$	$E^{\text{(NIST)}}$
$5d\ ^2D_{3/2}$	0	0	0	0	0	0
$5d\ ^2D_{5/2}$	8590	7822	9014	8596	8615	8709
$6s\ ^2S_{1/2}$	80126	77403	79316	80240	79575	79431
$6p\ ^2P_{1/2}$	149554	143590	148529	148424	147380	147553
$6p\ ^2P_{3/2}$	164130	159851	166290	165788	164931	165037
$6d\ ^2D_{3/2}$	262496	253853	263467	262356	261739	261695
$6d\ ^2D_{5/2}$	264750	256434	266207	265037	264455	264412
$7s\ ^2S_{1/2}$	280754	270152	280475	279285	278951	278916
$5f\ ^2F_{5/2}$	264659	259037	264343	263810	262150	261681
$5f\ ^2F_{7/2}$	265471	259261	265045	264359	262802	262430
$7p\ ^2P_{1/2}$	311630	298592	309470	308012	307589	
$7p\ ^2P_{3/2}$	317895	305687	317080	315499	315106	
$7d\ ^2D_{5/2}$	362631	349354	361768	360015	359634	
$7d\ ^2D_{5/2}$	362631	350621	363103	361323	360954	
$5g\ ^2G_{7/2}$	362615	351241	364554	362594	362290	362234
$5g\ ^2G_{9/2}$	362627	351222	364545	362581	362280	362222
$6f\ ^2F_{5/2}$	356115	349601	359287	357320	352557	
$6f\ ^2F_{7/2}$	359822	349790	359930	357946	353062	
$8s\ ^2S_{1/2}$	370410	356410	369224	367384	367130	
$6g\ ^2G_{7/2}$	412182	399541	413510	411364	411101	411087
$6g\ ^2G_{9/2}$	412192	399524	413502	411353	411094	411079
Ion. pot.		509850	525070	. 522585	522406	522370

excited $4f^{14}5p^56s^2$, $4f^{14}5p^55d6s$, and $4f^{14}5p^55d6p$ configurations are only partially autoionizing as some of the levels have energies below the ionization potential. Finally, none of the levels of the $4f^{14}5p^55d^2$, $4f^{13}5p^65d^2$, $4f^{13}5p^66s^2$, $4f^{13}5p^65d6s$, and $4f^{13}5p^65d6p$ configurations can autoionize.

During the radiative-stabilization phase of DR, dielectronic satellite lines are emitted when an electron jumps from a doubly-excited autoionizing state to a singly- and doubly-excited bound state. For instance, the radiative transitions in Tm-like tungsten from the $4f^{13}5p^6n'l'nl$ and $4f^{14}5p^5n'l'nl$ states to the $4f^{14}5p^6nl$ states give rise to satellite lines of the $4f - nl$ ($4f^{13}5p^6nl - 4f^{14}5p^6$) and $5p - nl$ ($4f^{14}5p^5nl - 4f^{14}5p^6$) lines of Er-like tungsten. Assuming a Maxwellian distribution, the effective emission rate coefficient of the dielectronic satellite line can be written as (see, for example, Ref. [38])

$$C_S^{\text{eff}}(j,i) = 3.3 \times 10^{-24} \left(\frac{I_H}{kT_e}\right)^{3/2} \frac{Q_d(j,i)}{g_0}$$
$$\times \exp\left(-\frac{E_S(i)}{kT_e}\right) \text{photons cm}^3\text{s}^{-1}, \quad (2)$$

where the intensity factor $Q_d(j,i)$ is defined as

$$Q_d(j,i) = \frac{g(i)A_a(i,i_0)A_r(j,i)}{\sum_{i_0'} A_a(i,i_0') + \sum_k A_r(k,i)}, \quad (3)$$

I_H is the ionization potential of hydrogen, j is the lower bound state, i is the upper autoionizing state, i_0 is the initial state (i.e., the ground state $4f^{14}5p^6$ of the Er-like ion), and i_0' is the possible final state for autoionization (again, only $4f^{14}5p^6$ in this case). The statistical weight of the initial state i_0 is

$g_0 = 1$, $g(i)$ is the statistical weight of the doubly-excited state, $A_a(i,i_0)$ is the autoionization rate from i to i_0, $A_r(j,i)$ is the radiative transition probability from i to j, $E_S(i)$ is the excitation energy of the autoionizing state i relative to the energy of $4f^{14}5p^6$, and T_e is the electron temperature. For some cases, $A_a \gg A_r$ and Q_d can be estimated as $Q_d(j,i) \approx g(i)A_r(j,i)$.

It follows from Eq. (2) that the intensity of dielectronic satellites depends on the intensity factor $Q_d(j,i)$ and excitation energy $E_S(i)$. The strongest lines with $Q_d(j,i) > 1.0 \times 10^{12}$ s^{-1} are presented in Tables IV and V for even- and odd-parity initial states, respectively. In these two tables, we present results for transitions from the $4f^{14}5p^5n'l'nl$ doubly-excited states; i.e., the $4f^{14}5p^5n'l'nl$-$4f^{14}5p^6nl$ transitions. In Tables VI and VII, we list transitions from the doubly-excited states with $4f$ hole; i.e., the $4f^{13}5p^6n'l'nl$-$4f^{14}5p^6nl$ transitions. The intensity factors $Q_d(j,i)$ for the strongest transitions given in Tables VI and VII are smaller than the intensity factors $Q_d(j,i)$ for transitions listed in two previous tables by a factor of 10. The values of the excitation energy $E_S(i)$ are similar in Tables IV, V and Tables VI, VII. As a result, values of the effective emission rate coefficients $C_S^{\text{eff}}(j,i)$ for the $4f^{13}5p^6n'l'nl$-$4f^{14}5p^6nl$ transitions are smaller by a factor of 10 than the $C_S^{\text{eff}}(j,i)$ values for the $4f^{14}5p^5n'l'nl$-$4f^{14}5p^6nl$ transitions.

Since the sum over the final states of autoionization i_0' in Eq. (3) includes only one state, $4f^{14}5p^6$, it is in fact reduced to a single rate $A_a(i)$. In addition to the $A_a(i)$ values, Tables IV–VII also present $E_S(i)$, weighted radiative rates $g_iA_r(j,i)$, sums of weighted radiative rates $\sum_k g_iA_r(k,i)$, wavelengths λ for dipole-allowed transitions, relative intensity factors $Q_d(j,i)$, and effective emission rate coefficients $C_S^{\text{eff}}(j,i)$. Abbreviated notations are used in these tables and in

TABLE III. Wavelengths (λ in Å), weighted oscillator strengths (gf), and weighted transition rates (gA_r) for the $4f^{14}5p^6nl$ and $4f^{14}5p^6n'l'$ transitions in Tm-like tungsten. Oscillator strengths and transition rates are calculated to the first, second, third, and all orders of RMBPT as well as HFR approximation (COWAN code). SD all-order values are given as recommended values where NIST data [19] are not available and are marked by as asterisk. $A[B]$ means $A \times 10^B$.

Transitions		λ (in Å)	Oscillator strengths (gf)					Transition rates (gA_r in s^{-1})				
nl, LSJ	nl, LSJ	Recom.	COWAN	DF	DF+2	DF+2+3	SD	COWAN	DF	DF+2	DF+2+3	DF+SD
$5d\,^2D_{3/2}$	$6f\,^2F_{5/2}$	283.642*	0.496	0.837	0.097	0.063	0.055	4.11[10]	6.94[10]	8.00[09]	5.21[09]	4.55[09]
$5d\,^2D_{5/2}$	$6f\,^2F_{7/2}$	290.826*	0.032	1.173	0.215	0.170	0.023	2.51[09]	9.25[10]	1.69[10]	1.34[10]	1.85[09]
$5d\,^2D_{5/2}$	$6f\,^2F_{5/2}$	290.826*	0.088	0.059	0.010	0.005	0.006	6.94[09]	4.63[09]	7.80[08]	4.19[08]	5.02[08]
$5d\,^2D_{3/2}$	$7p\,^2P_{3/2}$	317.354*	0.006	0.017	0.010	0.008	0.008	4.16[08]	1.12[09]	6.49[08]	5.46[08]	5.10[08]
$5d\,^2D_{3/2}$	$7p\,^2P_{1/2}$	325.109*	0.058	0.078	0.029	0.022	0.023	3.66[09]	4.90[09]	1.82[09]	1.42[09]	1.46[09]
$5d\,^2D_{5/2}$	$7p\,^2P_{3/2}$	326.374*	0.056	0.153	0.089	0.074	0.072	3.55[09]	9.59[09]	5.58[09]	4.62[09]	4.51[09]
$5d\,^2D_{3/2}$	$5f\,^2F_{5/2}$	382.145	1.798	3.862	1.918	2.012	2.008	8.21[10]	1.76[11]	8.76[10]	9.19[10]	9.17[10]
$5d\,^2D_{5/2}$	$5f\,^2F_{7/2}$	394.134	2.722	5.693	3.063	3.275	3.195	1.17[11]	2.44[11]	1.32[11]	1.41[11]	1.37[11]
$5d\,^2D_{5/2}$	$5f\,^2F_{5/2}$	395.301	0.131	0.286	0.152	0.155	0.154	5.59[09]	1.22[10]	6.49[09]	6.63[09]	6.55[09]
$6s\,^2S_{1/2}$	$7p\,^2P_{3/2}$	424.314*	0.017	0.001	0.025	0.015	0.012	6.09[08]	3.34[07]	9.37[08]	5.45[08]	4.61[08]
$6s\,^2S_{1/2}$	$7p\,^2P_{1/2}$	438.293*	0.009	0.009	0.049	0.040	0.036	2.89[08]	3.16[08]	1.69[09]	1.38[09]	1.27[09]
$5d\,^2D_{3/2}$	$6p\,^2P_{3/2}$	605.926	0.136	0.147	0.121	0.117	0.119	2.47[09]	2.67[09]	2.20[09]	2.12[09]	2.17[09]
$5d\,^2D_{5/2}$	$6p\,^2P_{3/2}$	639.683	1.176	1.399	1.159	1.121	1.145	1.92[10]	2.28[10]	1.89[10]	1.83[10]	1.87[10]
$5d\,^2D_{3/2}$	$6p\,^2P_{1/2}$	677.722	0.614	0.818	0.623	0.617	0.631	8.91[09]	1.19[10]	9.04[09]	8.95[09]	9.16[09]
$5f\,^2F_{5/2}$	$6g\,^2G_{7/2}$	669.317	0.935	1.210	0.841	0.934	0.929	1.40[10]	1.80[10]	1.25[10]	1.39[10]	1.38[10]
$5f\,^2F_{7/2}$	$6g\,^2G_{9/2}$	672.726	1.207	1.553	1.083	1.197	1.194	1.78[10]	2.29[10]	1.60[10]	1.76[10]	1.76[10]
$5f\,^2F_{7/2}$	$6g\,^2G_{7/2}$	672.689	0.034	0.044	0.031	0.034	0.034	5.08[08]	6.55[08]	4.57[08]	5.04[08]	5.01[08]
$6p\,^2P_{1/2}$	$7s\,^2S_{1/2}$	761.253	0.539	0.390	0.440	0.403	0.398	6.20[09]	4.49[09]	5.07[09]	4.63[09]	4.58[09]
$6p\,^2P_{3/2}$	$7s\,^2S_{1/2}$	878.127	0.933	1.053	1.114	1.056	1.045	8.06[09]	9.11[09]	9.64[09]	9.14[09]	9.04[09]
$6p\,^2P_{1/2}$	$6d\,^2D_{3/2}$	876.106	2.656	2.816	2.307	2.278	2.307	2.31[10]	2.45[10]	2.01[10]	1.98[10]	2.00[10]
$6p\,^2P_{3/2}$	$6d\,^2D_{5/2}$	1006.289	4.176	5.154	4.261	4.235	4.280	2.76[10]	3.39[10]	2.81[10]	2.79[10]	2.82[10]
$5f\,^2F_{5/2}$	$5g\,^2G_{7/2}$	994.500	7.107	8.560	7.421	6.530	6.439	4.79[10]	5.77[10]	5.00[10]	4.40[10]	4.34[10]
$5f\,^2F_{7/2}$	$5g\,^2G_{9/2}$	1002.084	9.259	11.082	9.614	8.568	8.446	6.15[10]	7.36[10]	6.39[10]	5.69[10]	5.61[10]
$5f\,^2F_{7/2}$	$5g\,^2G_{7/2}$	1001.964	0.265	0.316	0.275	0.245	0.241	1.76[09]	2.10[09]	1.82[09]	1.63[09]	1.60[09]
$6p\,^2P_{3/2}$	$6d\,^2D_{3/2}$	1034.577	0.452	0.570	0.469	0.467	0.472	2.82[09]	3.55[09]	2.92[09]	2.91[09]	2.94[09]
$6d\,^2D_{5/2}$	$6f\,^2F_{7/2}$	1134.490*	3.360	4.665	4.427	4.894	3.598	1.75[10]	2.42[10]	2.29[10]	2.54[10]	1.86[10]
$6d\,^2D_{3/2}$	$6f\,^2F_{5/2}$	1100.565*	2.496	3.109	2.959	3.346	2.473	1.37[10]	1.71[10]	1.63[10]	1.84[10]	1.36[10]
$6d\,^2D_{5/2}$	$6f\,^2F_{5/2}$	1134.490*	0.173	0.236	0.224	0.252	0.184	8.94[08]	1.22[09]	1.16[09]	1.30[09]	9.54[08]
$6s\,^2S_{1/2}$	$6p\,^2P_{3/2}$	1168.151	1.573	2.041	1.450	1.482	1.521	7.69[09]	9.98[09]	7.09[09]	7.24[09]	7.43[09]
$6s\,^2S_{1/2}$	$6p\,^2P_{1/2}$	1467.959	0.628	0.824	0.573	0.590	0.606	1.95[09]	2.55[09]	1.77[09]	1.82[09]	1.87[09]
$6d\,^2D_{3/2}$	$7p\,^2P_{3/2}$	1872.259*	0.251	0.255	0.256	0.242	0.242	4.77[08]	4.86[08]	4.87[08]	4.61[08]	4.61[08]
$6d\,^2D_{5/2}$	$7p\,^2P_{3/2}$	1972.608*	2.149	2.362	2.352	2.231	2.239	3.69[09]	4.05[09]	4.03[09]	3.82[09]	3.84[09]
$6d\,^2D_{3/2}$	$7p\,^2P_{1/2}$	2178.915*	1.198	1.330	1.302	1.245	1.248	1.69[09]	1.87[09]	1.83[09]	1.75[09]	1.75[09]
$7s\,^2S_{1/2}$	$7p\,^2P_{3/2}$	2763.156*	2.190	2.508	2.313	2.262	2.284	1.92[09]	2.19[09]	2.02[09]	1.98[09]	2.00[09]
$7s\,^2S_{1/2}$	$7p\,^2P_{1/2}$	3487.541*	0.961	1.036	0.949	0.929	0.938	5.27[08]	5.68[08]	5.20[08]	5.10[08]	5.14[08]

the text below: $4f^{14}5p^6nl = nl$, $4f^{13}5p^6nln'l' = 4fnln'l'$, and $4f^{14}5p^5nln'l' = 5pnln'l'$. The restriction $Q_d(j,i) > 5.0 \times 10^{12}$ s^{-1} leaves only a few dozen lines out of the total of 2.0×10^6 transitions, and most of these lines are due to the one-electron $5l$-$5p5lns$, $5l$-$5p5lnd$, $6l$-$5p6lns$, $6l$-$5p6lnd$, $5l$-$4f5lnd$, $5l$-$4f5lng$, and $6l$-$4f6lnd$ transitions with $l = s,p,d,f,g$.

Tables V–VII illustrate that there are a lot of transitions from nonautoionizing doubly-excited states, which is not the case for the Na-like W^{53+} [5], where only singly-excited states are nonautionozing and all of the doubly-excited states are autoionizing. To the contrary, in the case of Ag-like W^{27+}, a very large number of doubly-excited nonautoionizing states exist (about 2000 states) [2].

The strong mixing between some of configurations of doubly-excited states was already underlined in Refs. [2,5].

There is a lot of mixing between some of the configurations in W^{5+} as well. This effect is exemplified by $6d\,^2D_{3/2}$–$4f6s7s\,^2F^b_{5/2}$ and $6d\,^2D_{5/2}$–$4f6s7s\,^2F^b_{5/2}$ transitions in Table VI. The large intensity factors Q_d for these transitions are due to the mixing between the $4f^{13}5p^66s7s$ and $4f^{13}5p^66d7d$ configurations. However, a large value of Q_d is *per se* insufficient to guarantee a large effective rate coefficient as the $\exp[-E_s(i)/kT_e]$ factor may strongly modify it. Indeed, the C_S^{eff} coefficient for the $6s\,^2S_{1/2}$–$5p6s5d\,^2P^a_{1/2}$ transition (Table IV) is larger than the C_S^{eff} of the $7g\,^2G_{7/2}$–$5p5d7g\,^2F^a_{5/2}$ transition by a factor of 5.3, although the value of Q_d for the former transition is smaller (by a factor of 2) than that for the latter.

Figure 1 shows the dielectronic satellite spectra for an electron temperature $T_e = 20$ eV due to $[4f^{14}5p^55l'nl + 4f^{14}5p^56l''nl + 4f^{13}5p^65l'nl + 4f^{13}5p^66l''nl] \Rightarrow [4f^{14}$

TABLE IV. Autoionization rates (A_a in s^{-1}) and excitation energies (E_S in eV) for the odd-parity $4f^{14}5p^5nln'l'$ states. Wavelengths (λ in Å), weighted radiative rates (gA_r in s^{-1}), intensity factors (Q_d in s^{-1}) and effective emission rate coefficients (C_S^{eff} in cm^3/s) for transitions between the $4f^{14}5p^6nl$ even-parity excited and the $4f^{14}5p^5nln'l'$ odd-parity autoionization states of Tm-like tungsten. The C_S^{eff} values are given for $T_e = 20$ eV. Designations: $4f^{14}5p^6nl = nl$ and $4f^{14}5p^5nln'l' = 5pnln'l'$. The upper indices are used in the COWAN code to differentiate between atomic terms. $A[B]$ means $A \times 10^B$.

Lower level $nl\ LSJ$	Upper level $5pnln'l'\ LSJ$	A_a (s^{-1})	E_S (eV)	ΣgA_r (s^{-1})	gA_r (s^{-1})	λ (Å)	Q_d (s^{-1})	C_S^{eff} (cm^3/s)
$5d\ ^2D_{5/2}$	$5p5d6d\ ^2F^e_{7/2}$	4.37[13]	11.994	2.10[11]	1.60[11]	163.79	1.60[11]	1.63[−13]
$5d\ ^2D_{5/2}$	$5p5d6d\ ^4P^b_{5/2}$	1.43[13]	11.677	1.74[11]	1.36[11]	164.48	1.36[11]	1.40[−13]
$6d\ ^2D_{5/2}$	$5p5d6d\ ^2F^a_{7/2}$	3.37[14]	24.837	2.69[12]	2.68[12]	218.37	2.68[12]	1.43[−12]
$6s\ ^2S_{1/2}$	$5p6s5d\ ^2P^a_{3/2}$	1.54[14]	1.893	1.40[12]	1.37[12]	218.57	1.36[12]	2.29[−12]
$7s\ ^2S_{1/2}$	$5p7s5d\ ^2P^a_{3/2}$	1.19[14]	26.728	1.50[12]	1.48[12]	218.73	1.47[12]	7.15[−13]
$7s\ ^2S_{1/2}$	$5p7s5d\ ^2P^a_{1/2}$	1.06[14]	26.723	7.66[11]	7.39[11]	218.74	7.36[11]	3.58[−13]
$6d\ ^2D_{3/2}$	$5p5d6d\ ^2F^a_{5/2}$	1.33[14]	24.405	2.04[12]	1.84[12]	218.96	1.84[12]	1.00[−12]
$6s\ ^2S_{1/2}$	$5p6s5d\ ^2P^a_{1/2}$	1.22[14]	1.752	7.17[11]	6.81[11]	219.12	6.79[11]	1.15[−12]
$7g\ ^2G_{7/2}$	$5p5d7g\ ^2F^a_{5/2}$	2.27[13]	46.486	8.38[11]	1.21[12]	219.56	1.20[12]	2.17[−13]
$7g\ ^2G_{7/2}$	$5p5d7g\ ^2H^a_{9/2}$	7.36[13]	46.488	2.17[12]	1.58[12]	219.56	1.58[12]	2.86[−13]
$6g\ ^2G_{7/2}$	$5p5d6g\ ^2F^a_{5/2}$	4.33[11]	42.769	3.17[11]	1.27[12]	219.71	1.13[12]	2.46[−13]
$7g\ ^2G_{9/2}$	$5p5d7g\ ^2G^a_{9/2}$	1.72[13]	46.449	8.00[11]	1.41[12]	219.71	1.40[12]	2.54[−13]
$7d\ ^2D_{5/2}$	$5p5d7d\ ^2P^a_{3/2}$	2.59[12]	36.622	1.24[12]	1.16[12]	219.72	1.04[12]	3.08[−13]
$6g\ ^2G_{9/2}$	$5p5d6g\ ^2H^a_{11/2}$	6.06[13]	42.740	2.38[12]	2.34[12]	219.83	2.34[12]	5.11[−13]
$6g\ ^2G_{7/2}$	$5p5d6g\ ^2H^a_{9/2}$	5.26[13]	42.722	2.00[12]	1.99[12]	219.90	1.98[12]	4.33[−13]
$7d\ ^2D_{5/2}$	$5p5d7d\ ^2F^a_{7/2}$	1.58[14]	36.556	2.15[12]	1.77[12]	219.98	1.76[12]	5.24[−13]
$7g\ ^2G_{9/2}$	$5p5d7g\ ^2H^a_{11/2}$	2.68[13]	46.368	2.73[12]	2.45[12]	220.03	2.43[12]	4.43[−13]
$7g\ ^2G_{9/2}$	$5p5g6s\ ^2H^b_{9/2}$	7.80[12]	46.357	1.47[12]	1.13[12]	220.07	1.11[12]	2.02[−13]
$5g\ ^2G_{9/2}$	$5p5d5g\ ^2F^a_{7/2}$	1.53[13]	36.460	1.81[12]	1.20[12]	220.36	1.18[12]	3.53[−13]
$7d\ ^2D_{5/2}$	$5p5d7d\ ^2D^a_{5/2}$	1.45[12]	36.452	3.11[11]	1.26[12]	220.39	1.22[12]	3.65[−13]
$5g\ ^2G_{9/2}$	$5p5d5g\ ^2H^a_{11/2}$	1.13[14]	36.309	3.10[12]	2.98[12]	220.95	2.97[12]	8.95[−13]
$5g\ ^2G_{7/2}$	$5p5d5g\ ^2H^a_{9/2}$	6.28[13]	36.291	2.11[12]	1.80[12]	221.01	1.79[12]	5.40[−13]
$5g\ ^2G_{9/2}$	$5p5d5g\ ^2G^a_{9/2}$	1.62[11]	36.230	5.87[11]	1.30[12]	221.26	9.53[11]	2.88[−13]
$7s\ ^2S_{1/2}$	$5p7s5d\ ^4D_{3/2}$	2.59[13]	16.803	2.90[11]	2.42[11]	265.15	2.41[11]	1.92[−13]

$5p^6nl + 4f^{14}5p^56s^2 + 4f^{14}5p^55d6s + 4f^{14}5p^55d6p + 4f^{14}5p^55d^2 + 4f^{13}5p^65d^2 + 4f^{13}5p^66s^2 + 4f^{13}5p^65d6s + 4f^{13}5p^65d6p$] transitions (total of 3200 transitions). We noted above that the doubly-excited $4f^{14}5p^56s^2$, $4f^{14}5p^55d6s$, and $4f^{14}5p^55d6p$ configurations are only partially autoionizing. This means that some of these levels have energies below or above the ionization potential (for example, among the 65 levels of the $4f^{14}5p^55d6p$ configuration, the 28 levels are above the ionization potential, while the 37 levels are under ionization potential). The effective emission rate coefficients $C_S^{\text{eff}}(j,i)$ and Gaussian profiles with spectral resolution $R \equiv \lambda/\Delta\lambda = 400$–$3000$ are used to synthesize these spectra and to highlight the specific spectral features. The limited set of transitions includes transitions with 10^{-14} cm^3/s $< C_S^{\text{eff}}(j,i) < 2.3 \times 10^{-12}$ cm^3/s.

The strongest lines shown in the top right panel of Fig. 1 result from the $6d\ ^2D_{5/2}$–$5p5d6d\ ^2F^a_{7/2}$, $6s\ ^2S_{1/2}$–$5p6s5d\ ^2P^a_{3/2}$, $6d\ ^2D_{3/2}$–$5p5d6d\ ^2F^a_{5/2}$, and $6s\ ^2S_{1/2}$–$5p6s5d\ ^2P^a_{1/2}$ transitions with wavelengths λ equal to 218.37 Å, 218.57 Å, 218.96 Å, and 219.12 Å, respectively. Those four lines are the satellite lines to the strong $\lambda = 216.219$ Å line of the $4f^{14}5p^6\ ^1S_0$–$4d^{14}5p^55d\ ^1P_1$ resonance transitions in Er-like tungsten [19]. The satellite lines to another resonance strong line in the Er-like tungsten at $\lambda = 261.387$ Å [19]

($4f^{14}5p^6\ ^1S_0$–$4d^{14}5p^55d\ ^3D_1$ transition) are shown in the bottom left panel of Fig. 1. The strongest satellite lines correspond to the $5f\ ^2F_{7/2}$–$5p5d5f\ ^4P^a_{5/2}$ transition ($\lambda = 262.89$ Å) and $5f\ ^2F_{5/2}$–$5p5d5f\ ^2P^c_{3/2}$ transition ($\lambda = 262.91$ Å). The strongest lines shown in the top left panel of Fig. 1 are due to the $5d\ ^2D_{5/2}$–$5p5d6d\ ^2F^e_{7/2}$ ($\lambda = 163.79$ Å) and $5d\ ^2D_{5/2}$–$5p5d6d\ ^4P^b_{5/2}$ ($\lambda = 164.48$ Å) transitions.

The large number of strongest lines shown in the bottom left panel of Fig. 1 results from the transitions between the nonautoionizing ($4f5d^2 + 4f5d6p + 4f5d6s$) doubly-excited states and the autoionizing ($4f5d5f + 4f6p5f + 4f6s5f$) doubly-excited states.

In particular, the wavelengths of the more than 2000 transitions ($4f5d^2$-$4f5d5f$, $4f5d6p$-$4f6p5f$, and $4f5d6s$-$4f5f6s$) are distributed in the region of 335–380 Å. The values of effective emission rate coefficient C_S^{eff} are about 1–700 in units of 10^{-15} cm^3/s.

Synthetic spectra of the DR satellite shown in the bottom right panel of Fig. 1 give another example of the contribution of transitions between the doubly-excited states. The strongest lines around $\lambda = 405$ Å are due to the $5p5d^2$-$5p5d5f$ transitions, and around $\lambda = 550$ Å are due to the $4f5d6p$-$4f6p^2$ and $4f5d6s$-$4f6s6p$ transitions. The strongest lines around

TABLE V. Autoionization rates (A_a in s^{-1}) and excitation energies (E_S in eV) for the even-parity $4f^{14}5p^5nln'l'$ states. Wavelengths (λ in Å), weighted radiative rates (gA_r in s^{-1}), intensity factors (Q_d in s^{-1}), and effective emission rate coefficients (C_S^{eff} in cm^3/s) for transitions between the $4f^{14}5p^6nl$ odd-parity excited and the $4f^{14}5p^5nln'l'$ even-parity autoionization states of Tm-like tungsten. The C_S^{eff} values are given for $T_e = 20$ eV. Designations: $4f^{14}5p^6nl = nl$ and $4f^{14}5p^5nln'l' = 5pnln'l'$. The upper indices are used in the COWAN code to differentiate between atomic terms. $A[B]$ means $A \times 10^B$.

Lower level $nl\ LSJ$	Upper level $5pnln'l'\ LSJ$	A_a (s^{-1})	E_S (eV)	ΣgA_r (s^{-1})	gA_r (s^{-1})	λ (Å)	Q_d (s^{-1})	C_S^{eff} (cm^3/s)
$6f\ ^2F_{5/2}$	$5p5d6f\ ^2G_{7/2}^a$	2.31[14]	36.141	2.38[12]	1.15[12]	217.22	1.14[12]	3.46[−13]
$5f\ ^2F_{7/2}$	$5p5d5f\ ^2D_{5/2}^a$	4.93[13]	25.153	2.43[12]	1.93[12]	217.50	1.91[12]	1.00[−12]
$5p5d^2\ ^2F_{5/2}$	$5p5d7f\ ^2G_{7/2}^a$	1.42[14]	42.523	2.46[12]	8.74[11]	217.59	8.72[11]	1.92[−13]
$5f\ ^2F_{7/2}$	$5p5d5f\ ^2G_{9/2}^a$	4.77[14]	25.012	3.02[12]	2.41[12]	218.04	2.41[12]	1.28[−12]
$6f\ ^2F_{7/2}$	$5p5d6f\ ^2G_{9/2}^a$	3.06[14]	36.357	2.95[12]	1.74[12]	218.68	1.74[12]	5.23[−13]
$6p\ ^2P_{3/2}$	$5p5d6p\ ^2P_{3/2}^a$	2.22[13]	12.225	1.17[12]	1.10[12]	218.89	1.08[12]	1.08[−12]
$6p\ ^2P_{3/2}$	$5p5d6p\ ^2D_{5/2}^a$	4.09[14]	12.195	1.18[12]	9.94[11]	219.01	9.94[11]	1.00[−12]
$5f\ ^2F_{7/2}$	$5p5d5f\ ^2F_{7/2}^a$	2.30[13]	24.731	2.96[12]	2.63[12]	219.12	2.59[12]	1.39[−12]
$6f\ ^2F_{7/2}$	$5p5d6f\ ^2F_{7/2}^a$	1.04[12]	36.243	4.09[11]	1.58[12]	219.12	1.50[12]	4.53[−13]
$7f\ ^2F_{7/2}$	$5p5d7f\ ^2D_{5/2}^a$	1.55[13]	42.683	1.86[12]	1.11[12]	219.21	1.09[12]	2.39[−13]
$7f\ ^2F_{7/2}$	$5p5d7f\ ^2G_{9/2}^a$	2.12[14]	42.637	3.06[12]	1.96[12]	219.39	1.95[12]	4.28[−13]
$7f\ ^2F_{7/2}$	$5p5d7f\ ^2F_{7/2}^a$	1.64[13]	42.572	2.46[12]	1.66[12]	219.64	1.63[12]	3.59[−13]
$5p6s5d\ ^4F_{7/2}$	$5p5d7f\ ^2G_{9/2}^a$	2.12[14]	42.637	3.06[12]	6.62[11]	219.90	6.61[11]	1.45[−13]
$5p6s5d\ ^4F_{7/2}$	$5p5d7f\ ^2F_{7/2}^a$	1.64[13]	42.572	2.46[12]	5.64[11]	220.15	5.53[11]	1.22[−13]
$7p\ ^2P_{1/2}$	$5p5d7p\ ^2D_{3/2}^a$	8.88[13]	30.019	1.18[12]	1.16[12]	220.22	1.15[12]	4.74[−13]
$5f\ ^2F_{5/2}$	$5p5d5f\ ^2G_{7/2}^a$	3.59[14]	24.308	2.52[12]	2.16[12]	220.38	2.16[12]	1.19[−12]
$7p\ ^2P_{3/2}$	$5p5d7p\ ^2D_{5/2}^a$	8.25[13]	30.734	1.05[12]	1.00[12]	220.56	9.99[11]	3.98[−13]
$7p\ ^2P_{3/2}$	$5p5d7p\ ^2P_{3/2}^a$	2.29[13]	30.735	1.12[12]	1.09[12]	220.56	1.08[12]	4.30[−13]
$7f\ ^2F_{5/2}$	$5p5d7f\ ^2G_{7/2}^a$	1.42[14]	42.523	2.46[12]	1.37[12]	223.74	1.36[12]	3.00[−13]
$5p5d^2\ ^2G_{7/2}$	$5p5d6f\ ^2G_{9/2}^a$	3.06[14]	36.357	2.95[12]	7.43[11]	224.37	7.42[11]	2.23[−13]
$5p5d^2\ ^2F_{5/2}$	$5p5d6f\ ^2G_{7/2}^a$	2.31[14]	36.141	2.38[12]	8.76[11]	224.53	8.75[11]	2.66[−13]
$5p5d^2\ ^2G_{7/2}$	$5p5d6f\ ^2F_{7/2}^a$	1.04[12]	36.243	4.09[11]	6.07[11]	224.84	5.78[11]	1.75[−13]
$5p6s5d\ ^4F_{7/2}$	$5p6s5f\ ^4G_{9/2}$	3.32[11]	21.906	4.25[11]	2.95[11]	351.48	2.62[11]	1.62[−13]
$5p6s5d\ ^2F_{7/2}^b$	$5p6s5f\ ^2G_{9/2}^b$	1.54[13]	22.714	5.72[11]	3.68[11]	353.85	3.67[11]	2.18[−13]
$5p6s5d\ ^2F_{7/2}^a$	$5p6s5f\ ^2G_{9/2}^a$	3.88[12]	32.367	6.09[11]	3.86[11]	358.89	3.80[11]	1.39[−13]
$5p5d^2\ ^4G_{11/2}$	$5p5d5f\ ^4H_{13/2}^b$	2.74[11]	10.013	5.93[11]	4.99[11]	363.84	4.32[11]	4.85[−13]
$5p5d^2\ ^2H_{11/2}$	$5p5d5f\ ^2I_{13/2}^b$	5.23[10]	11.647	5.57[11]	8.14[11]	365.42	4.62[11]	4.78[−13]
$5p6s5d\ ^4D_{7/2}$	$5p6s5f\ ^4F_{9/2}$	1.04[11]	22.369	4.10[11]	3.38[11]	366.19	2.43[11]	1.47[−13]
$5p5d^2\ ^2G_{9/2}$	$5p5d5f\ ^2H_{11/2}^c$	2.77[12]	12.609	7.90[11]	7.44[11]	368.60	7.27[11]	7.16[−13]

$\lambda = 870$ Å are due to the $4f5d6p$-$4f5d6d$ transitions, while the strongest lines around $\lambda = 1006$ Å are due to the $5p5d6p$-$5p5d6d$ transitions.

IV. DIELECTRONIC RECOMBINATION RATE COEFFICIENTS FOR EXCITED STATES

The DR rate coefficients for excited states are obtained by summing the effective emission rate coefficients $C_S^{\text{eff}}(j,i)$ [Eq. (2)] for DR processes through all possible intermediate doubly-excited states:

$$\alpha_d(i_0, j) = \sum_i C_S^{\text{eff}}(j, i). \quad (4)$$

For the DR process described by Eq. (1), one has to calculate $\alpha_d(i_0, j)$ with $i_0 = 4f^{14}5p^6$ and all possible autoionizing doubly-excited states j of W^{27+} with energies larger than the $4f^{14}5p^6$ threshold $I_{\text{th}} = 522370$ cm^{-1} [19]. Among the doubly-excited $4f^{14}5p^55l'nl$ and $4f^{13}5p^65l'nl$ ($n = 5$–7) states, 4318 states of even parity and 4363 states of odd parity

have energies above I_{th}. The doubly-excited $4f^{14}5p^56l'nl$ and $4f^{13}5p^66l'nl$ ($n = 6$–7) configurations include 3798 levels of even parity and 3187 levels of odd parity.

The sum over i in Eq. (4) includes the $4f^{14}5p^55l'n_1l$ and $4f^{13}5p^65l'n_1l$, $4f^{14}5p^56l'n_2l$ and $4f^{13}5p^66l'n_2l$ doubly-excited, autoionizing states with $n_1 = 5$–7 (8681 levels) and $n_2 = 6$–7 (6985 levels). In Fig. 2, we illustrate the contributions of the $4f^{14}5p^55l'nl$, $4f^{13}5p^65l'nl$, $4f^{14}5p^56l'nl$, and $4f^{13}5p^66l'nl$ states to the DR rate coefficients $\alpha_d(4f^{14}5p^6, j)$ for the $j = 4f^{14}5p^6nl$ ^2L states as a function of T_e in Tm-like tungsten. The contributions from the autoionizing $4f^{14}5p^55l'nl$, $4f^{13}5p^65l'nl$, and $4f^{14}5p^56l'nl$, and $4f^{13}5p^66l'nl$ ($n = 5$–7) configurations are represented by curves 1, 2, 3, and 4, respectively (see Fig. 2). The largest contribution to the DR rate coefficient comes from the $4f^{14}5p^55l'nl$ channel (curve 1) for $j = 4f^{14}5p^65d$ ^2D and $j = 4f^{14}5p^66p$ ^2P states. The smallest contributions to $\alpha_d(4f^{14}5p^6, j)$ for $j = 4f^{14}5p^65d$ ^2D state (left panel of Fig. 2) are given by the $4f^{14}5p^56l'nl$ and $4f^{13}5p^66l'nl$ channels (curves 3 and 4), while the the $4f^{14}5p^56l'nl$

TABLE VI. Autoionization rates (A_a in s^{-1}) and excitation energies (E_S in eV) for the odd-parity $4f^{13}5p^6nln'l'$ states. Wavelengths (λ in Å), weighted radiative rates (gA_r in s^{-1}), intensity factors (Q_d in s^{-1}), and effective emission rate coefficients (C_S^{eff} in cm^3/s) for transitions between the $4f^{14}5p^6nl$ even-parity excited and the $4f^{13}5p^6nln'l'$ odd-parity autoionization states of Tm-like tungsten. The C_S^{eff} values are given for $T_e = 20$ eV. Designations: $4f^{14}5p^6nl = nl$ and $4f^{13}5p^6nln'l' = 4fnln'l'$. The upper indices are used in the COWAN code to differentiate between atomic terms. $A[B]$ means $A \times 10^B$.

Lower level $nl\ LSJ$	Upper level $4fnln'l'\ LSJ$	A_a (s^{-1})	E_S (eV)	ΣgA_r (s^{-1})	gA_r (s^{-1})	λ (Å)	Q_d (s^{-1})	C_S^{eff} (cm^3/s)
$6d\ ^2D_{3/2}$	$4f6s7s\ ^2F_{5/2}^b$	2.03[13]	24.649	4.59[11]	7.54[10]	218.02	7.51[10]	4.05[−14]
$6d\ ^2D_{5/2}$	$4f6s7s\ ^2F_{5/2}^b$	2.03[13]	24.649	4.59[11]	3.77[11]	219.09	3.75[11]	2.02[−13]
$5g\ ^2G_{9/2}$	$4f5d5g\ ^2F_{7/2}^a$	3.10[11]	21.506	1.50[11]	1.41[11]	298.89	1.33[11]	8.40[−14]
$5g\ ^2G_{7/2}$	$4f5d5g\ ^2F_{5/2}^a$	3.04[11]	21.502	9.51[10]	9.06[10]	298.91	8.61[10]	5.44[−14]
$5g\ ^2G_{9/2}$	$4f5d5g\ ^2H_{11/2}^a$	1.53[13]	21.502	2.04[11]	2.00[11]	298.93	2.00[11]	1.26[−13]
$6g\ ^2G_{9/2}$	$4f5d6g\ ^2F_{7/2}^a$	3.11[11]	27.660	1.06[11]	8.00[10]	298.94	7.67[10]	3.56[−14]
$5g\ ^2G_{7/2}$	$4f5d5g\ ^2G_{7/2}^a$	1.80[11]	21.494	1.58[11]	1.48[11]	298.97	1.34[11]	8.47[−14]
$6g\ ^2G_{7/2}$	$4f5d6g\ ^2H_{9/2}^a$	1.55[13]	27.653	1.75[11]	1.69[11]	298.99	1.68[11]	7.80[−14]
$5g\ ^2G_{9/2}$	$4f5d5g\ ^2G_{9/2}^a$	1.64[10]	21.492	1.90[11]	1.84[11]	299.00	8.51[10]	5.38[−14]
$6g\ ^2G_{9/2}$	$4f5d6g\ ^2H_{11/2}^a$	1.48[13]	27.652	2.04[11]	2.01[11]	299.00	2.00[11]	9.29[−14]
$6g\ ^2G_{9/2}$	$4f5d6g\ ^2G_{9/2}^a$	4.28[10]	27.647	1.70[11]	1.63[11]	299.04	1.16[11]	5.39[−14]
$7d\ ^2D_{5/2}$	$4f5d7d\ ^2F_{7/2}^a$	4.45[12]	21.358	3.13[10]	1.05[11]	300.22	1.05[11]	6.68[−14]
$7s\ ^2S_{1/2}$	$4f5d7s\ ^2P_{3/2}^a$	1.74[13]	11.096	1.08[11]	7.98[10]	301.78	7.97[10]	8.47[−14]
$6d\ ^2D_{5/2}$	$4f5d6d\ ^2F_{7/2}^a$	4.04[13]	9.172	1.14[11]	6.11[10]	302.08	6.11[10]	7.15[−14]
$6d\ ^2D_{3/2}$	$4f5d6d\ ^2F_{5/2}^a$	3.38[13]	8.880	1.11[11]	5.97[10]	302.21	5.97[10]	7.09[−14]
$6d\ ^2D_{5/2}$	$4f5d6d\ ^2D_{5/2}^a$	5.66[12]	8.687	9.73[10]	4.99[10]	305.69	4.97[10]	5.96[−14]
$4f5d6p\ ^2G_{7/2}^d$	$4f6p5f\ ^2H_{9/2}^d$	3.24[11]	33.934	5.35[11]	2.23[11]	332.89	1.91[11]	6.48[−14]
$4f5d6p\ ^4F_{9/2}^n$	$4f6p5f\ ^2H_{11/2}^f$	3.59[11]	31.868	6.68[11]	1.83[11]	334.49	1.59[11]	5.98[−14]
$4f5d6p\ ^2H_{9/2}^c$	$4f6p5f\ ^2I_{11/2}^d$	9.48[11]	34.046	6.68[11]	1.53[11]	335.54	1.44[11]	4.86[−14]
$4f6s6p\ ^2F_{5/2}^b$	$4f6p5f\ ^2G_{7/2}^e$	1.46[12]	34.553	3.20[11]	1.26[11]	336.37	1.22[11]	4.01[−14]
$4f5d6p\ ^4H_{9/2}^b$	$4f6p5f\ ^2H_{11/2}^a$	1.94[11]	30.776	6.17[11]	3.20[11]	341.31	2.53[11]	1.00[−13]
$4f5d6p\ ^4H_{9/2}^a$	$4f5d6d\ ^4I_{11/2}^a$	7.42[09]	5.782	8.85[10]	6.20[10]	874.19	3.11[10]	4.31[−14]
$4f5d6p\ ^4I_{9/2}$	$4f5d6d\ ^4K_{11/2}$	4.56[10]	6.735	8.35[10]	5.58[10]	883.12	4.84[10]	6.40[−14]
$4f5d6p\ ^2G_{7/2}^a$	$4f5d6d\ ^2H_{9/2}^a$	2.68[10]	6.907	7.05[10]	3.91[10]	884.29	3.10[10]	4.06[−14]
$4f5d6p\ ^2D_{5/2}^d$	$4f5d6d\ ^2F_{7/2}^f$	3.16[11]	4.420	5.53[10]	3.75[10]	893.45	3.66[10]	5.43[−14]
$4f5d6p\ ^2G_{9/2}^d$	$4f5d6d\ ^2H_{11/2}^a$	8.05[10]	8.182	6.92[10]	3.91[10]	1006.11	3.64[10]	4.47[−14]

channel (curve 3) gives the large contribution for the $j = 4f^{14}5p^66p\ ^2P$ state shown on the right panel of Fig. 2. We use an abbreviated notation to label the curves in Fig. 2: $5pn'l'nl$ instead of $4f^{14}5p^5n'l'nl$, $4fn'l'nl$ instead of $4f^{13}5p^6n'l'nl$, and nl instead of $4f^{14}5p^6nl$.

In order to estimate the contributions from the high-n autoionizing states to the DR rate coefficients associated with excited states, i.e., sum over i with $n > 7$ for $4f^{14}5p^65l'nl$, $4f^{13}5p^65l'nl$, $4f^{14}5p^66l'nl$, and $4f^{13}5p^66l'nl$ autoionizing states, we use empirical scaling laws [20], which can only be implemented to include one-electron $5p$-ns, $5p$-nd, $4f$-np, and $4f$-ng dipole transitions. The contributions from the high-n states appear for the first low-lying configurations $4f^{14}5p^65l$ and $4f^{14}5p^66l$. For these configurations, the $5l$-$5p5lns$, $5l$-$5p5lnd$, $6l$-$5p6lns$, $6l$-$5p6lnd$, $5l$-$4f5lnd$, $5l$-$4f5lng$, $6l$-$4f6lnd$, and $6l$-$4f6lng$ transitions with $n > 7$ and $l = s, p, d, f, g$ need to be included as well.

To estimate $Q_d(j,i)$ in Eq. (3) for autoionization states i with high principal quantum number n for the $5p5lnl'$, $5p6lnl'$, $4f5lnl'$, and $4f6lnl'$ configurations and for the $5p$-ns, $5p$-nd, $4f$-np, and $4f$-ng dipole transitions, we used our calculated data for $n = 7$ and the $1/n^3$ scaling law for rates A_a and A_r. For example, the formulas for the $5d$-$4f5dng$

case are

$$A_a(4f5dng\ ^{2,4}L_J) = \left(\frac{7}{n}\right)^3 A_a(4f5d7g\ ^{2,4}L_J), \quad (5)$$

$$A_r(5d\ ^2D_{3/2}\text{–}4f5dng\ ^{2,4}L_J)$$
$$= \left(\frac{7}{n}\right)^3 A_r(5d\ ^2D_{3/2}\text{–}4f5d7g\ ^{2,4}L_J)$$
$$\left(\frac{\Delta E(5d\ ^2D_{3/2}\text{–}4f5dng\ ^{2,4}L_J)}{\Delta E(5d\ ^2D_{3/2}\text{–}4f5d7g\ ^{2,4}L_J)}\right)^3. \quad (6)$$

In order to obtain the energies of the $4d5dnf\ ^{2,4}L_J$ states as functions of n, the following asymptotic formula is proposed (see Refs. [39,40]):

$$E(4f5dng)\text{–}E(4f5d) = -\frac{1}{2n^2}\left(Z - 60 + \frac{b(l)}{n}\right)^2, \quad (7)$$

where $b(l)$ is the l-dependent screening constant. Consequently, the energy differences in Tm-like W ($Z = 74$) can

TABLE VII. Autoionization rates (A_a in s^{-1}) and excitation energies (E_S in eV) for the even-parity $4f^{13}5p^6nln'l'$ states. Wavelengths (λ in Å), weighted radiative rates (gA_r in s^{-1}), intensity factors (Q_d in s^{-1}), and effective emission rate coefficients (C_S^{eff} in cm^3/s) for transitions between the $4f^{14}5p^6nl$ odd-parity excited and the $4f^{13}5p^6nln'l'$ even-parity autoionization states of Tm-like tungsten. The C_S^{eff} values are given for $T_e = 20$ eV. Designations: $4f^{14}5p^6nl = nl$ and $4f^{13}5p^6nln'l' = 4fnln'l'$. The upper indices are used in the COWAN code to differentiate between atomic terms. $A[B]$ means $A \times 10^B$.

Lower level nl LSJ	Upper level $4fnln'l'$ LSJ	A_a (s^{-1})	E_S (eV)	ΣgA_r (s^{-1})	gA_r (s^{-1})	λ (Å)	Q_d (s^{-1})	C_S^{eff} (cm^3/s)
$6p\ ^2P_{1/2}$	$4f5d5f\ ^2D_{3/2}^i$	1.67[13]	11.328	4.55[11]	2.79[11]	215.43	2.77[11]	2.91[−13]
$5f\ ^2F_{5/2}$	$4f5d5f\ ^2G_{7/2}^a$	2.67[13]	9.375	3.70[11]	4.75[10]	299.65	4.74[10]	5.49[−14]
$7f\ ^2F_{5/2}^k$	$4f5d7f\ ^2G_{7/2}^a$	3.37[13]	27.471	2.01[11]	1.35[11]	299.85	1.34[11]	6.28[−14]
$7f\ ^2F_{7/2}$	$4f5d7f\ ^2G_{9/2}^a$	3.91[13]	27.486	2.52[11]	1.20[11]	300.02	1.20[11]	5.62[−14]
$5f\ ^2F_{5/2}$	$4f5d5f\ ^2F_{5/2}^a$	1.04[12]	9.243	3.16[11]	6.80[10]	300.61	6.47[10]	7.54[−14]
$7p\ ^2P_{3/2}$	$4f5d7p\ ^2D_{5/2}^a$	1.78[13]	15.600	9.47[10]	3.85[10]	300.79	3.85[10]	3.27[−14]
$6f\ ^2F_{7/2}$	$4f5d6f\ ^2G_{9/2}^a$	5.59[13]	21.197	3.19[11]	1.83[11]	301.26	1.82[11]	1.17[−13]
$6f\ ^2F_{5/2}$	$4f5d6f\ ^2G_{7/2}^a$	4.79[13]	21.147	2.52[11]	1.33[11]	301.33	1.33[11]	8.55[−14]
$7p\ ^2P_{1/2}$	$4f5d7p\ ^2D_{3/2}^a$	1.50[13]	14.756	7.47[10]	4.68[10]	302.13	4.67[10]	4.13[−14]
$4f6s5d\ ^2H_{9/2}^a$	$4f6s5f\ ^2I_{11/2}^a$	2.21[10]	19.444	5.39[11]	5.01[11]	334.46	1.66[11]	1.16[−13]
$4f6s5d\ ^4H_{11/2}$	$4f6s5f\ ^4I_{13/2}$	2.18[10]	19.432	6.11[11]	4.97[11]	335.95	1.66[11]	1.16[−13]
$4f6s5d\ ^4H_{9/2}$	$4f6s5f\ ^4I_{11/2}$	4.62[10]	21.523	5.24[11]	3.40[11]	336.03	1.75[11]	1.10[−13]
$4f6s5d\ ^2H_{11/2}^b$	$4f6s5f\ ^2I_{13/2}^b$	5.62[11]	20.218	4.14[11]	2.88[11]	341.36	2.74[11]	1.85[−13]
$4f5d2\ ^2I_{11/2}$	$4f5d5f\ ^4K_{13/2}^a$	2.89[10]	6.291	7.41[11]	5.58[11]	345.75	1.97[11]	2.66[−13]
$4f5d2\ ^4I_{11/2}$	$4f5d5f\ ^4K_{13/2}^b$	1.80[11]	9.159	6.81[11]	3.54[11]	346.43	2.79[11]	3.27[−13]
$4f6s5d\ ^4G_{7/2}$	$4f6s5f\ ^4H_{9/2}$	9.01[10]	21.726	4.18[11]	2.43[11]	346.92	1.66[11]	1.04[−13]
$4f6s5d\ ^2G_{7/2}^b$	$4f6s5f\ ^2H_{9/2}^b$	1.98[12]	22.492	4.68[11]	2.48[11]	347.27	2.43[11]	1.46[−13]
$4f5d2\ ^2H_{11/2}$	$4f5d5f\ ^4I_{13/2}^a$	1.15[11]	9.645	2.40[11]	4.13[11]	353.80	3.60[11]	4.11[−13]
$5p6s5d\ ^4F_{9/2}$	$4f6s5f\ ^2H_{11/2}^a$	3.45[11]	21.857	5.11[11]	3.16[11]	354.62	2.81[11]	1.74[−13]
$4f5d2\ ^2G_{7/2}$	$5p5d5f\ ^2G_{9/2}^d$	6.46[12]	10.791	5.85[11]	3.04[11]	356.73	3.01[11]	3.25[−13]
$4f5d2\ ^2H_{11/2}$	$4f5d5f\ ^4H_{13/2}^a$	2.12[11]	7.646	6.86[11]	5.07[11]	356.77	4.12[11]	5.20[−13]
$4f5d2\ ^2I_{11/2}$	$4f5d5f\ ^2K_{13/2}^c$	4.06[11]	10.949	8.12[11]	7.23[11]	357.32	6.33[11]	6.78[−13]
$4f5d2\ ^2H_{9/2}$	$4f5d5f\ ^2I_{11/2}^e$	3.16[11]	11.041	8.41[11]	4.83[11]	359.79	3.95[11]	4.21[−13]
$4f5d2\ ^4G_{11/2}^k$	$4f5d5f\ ^2I_{13/2}^e$	3.51[11]	8.955	8.02[11]	2.97[11]	360.02	2.56[11]	3.03[−13]
$5p5d2\ ^4D_{7/2}$	$4f5d5f\ ^2H_{9/2}^e$	3.49[11]	9.725	4.59[11]	1.20[11]	362.09	1.06[11]	1.21[−13]
$4f5d2\ ^4G_{11/2}$	$4f5d5f\ ^4H_{13/2}^c$	5.23[10]	7.875	6.82[11]	3.96[11]	362.63	2.05[11]	2.56[−13]
$5p5d2\ ^2H_{9/2}$	$4f6s5f\ ^2I_{11/2}^b$	5.63[11]	22.360	6.03[11]	2.16[11]	363.74	1.98[11]	1.20[−13]

be found using the following formula:

$$\Delta E(5d\ ^2D_{3/2} - 4f5dng\ ^{2,4}L_J)$$
$$= \Delta E(5d\ ^2D_{3/2} - 4f5d7g\ ^{2,4}L_J) - \frac{196}{2}\left(\frac{1}{n^2} - \frac{1}{7^2}\right). \quad (8)$$

A similar formula was used for the excitation energies $E_S(i)$ in Eq. (4) for $i = 4f5dng\ ^{2,4}L_J$:

$$E_S(4f5dng\ ^{2,4}L_J)$$
$$= E_S(4f5d7g\ ^{2,4}L_J) - \frac{196}{2}\left(\frac{1}{n^2} - \frac{1}{7^2}\right). \quad (9)$$

Using these scaling formulas for $A_a(4f^{13}5p^65dng\ ^{2,4}L_J)$ and $A_r(4f^{14}5p^65d\ ^2D_{3/2} - 4f^{13}5dng\ ^{2,4}L_J)$, we calculated $Q_d(4f^{14}5p^65d\ ^2D_{3/2} - 4f^{13}5dng\ ^{2,4}L_J)$ as a function of n and then, using Eq. (9) for E_S, the sums over n for $\alpha_d(4f^{14}5p^6, 4f^{14}5p^65d\ ^2D_{3/2})$ versus T_e.

The results of the calculations for the $\alpha_d(4f^{14}5p^6, j)$ with $j = 4f^{14}5p^65d\ ^2D$ and $j = 4f^{14}5p^66p\ ^2P$ terms are shown in two panels of Fig. 2. The contribution of scaled data from $n = 8$ up to $n = 100$ (curve 5) for the

combined contributions from the autoionizing $4f^{14}5p^55l'nl$, $4f^{13}5p^65l'nl$ and $4f^{14}5p^56l'nl$, $4f^{13}5p^66l'nl$ configurations are presented by curve 5 (cf. curve labeled "scaled") in Fig. 2. The dependence of these results on the upper limit of n was also investigated. We found that there is a small difference for low temperature (1% for $T_e = 8$ eV) when $n = 20$ is taken to be the upper limit instead of $n = 100$. The difference increases for high temperatures reaching 15% for $T_e = 70$ eV. Scaled curves 5 give the largest contribution to $\alpha_d(4f^{14}5p^6, j)$ with $j = 4f^{14}5p^65d\ ^2D$ at $T_e = 32$ eV (left panel of Fig. 2) and at $T_e = 54$ eV for $j = 4f^{14}5p^66p\ ^2P$. The importance of these contributions is evident from both panels of Fig. 2.

The calculated values of $\alpha_d(4f^{14}5p^6, j)$ from Tm-like tungsten are plotted in Fig. 3 as a function of T_e. In the four panels, we present the DR rate coefficients $\alpha_d(4f^{14}5p^6, j)$ with $j = 4f^{14}5p^6ns\ ^2S$, $4f^{14}5p^6np\ ^2P$, $4f^{14}5p^6nd\ ^2D$, $4f^{14}5p^6nf\ ^2F$, and $4f^{14}5p^6ng\ ^2G$. The electron temperature for these plots varies from $T_e = 0.1$ eV to $T_e = 580$ eV. In order to decrease the number of curves shown, we summed the results for the doublets $[^2P_{1/2} + {}^2P_{3/2}]$, $[^2D_{3/2} + {}^2D_{5/2}]$, and $[^2F_{5/2} + {}^2F_{7/2}]$. In Fig. 3, the largest values of $\alpha_d(4f^{14}5p^6, j)$ with $j = 4f^{14}5p^66s\ ^2S$ and $4f^{14}5p^66p\ ^2F$ are obtained for
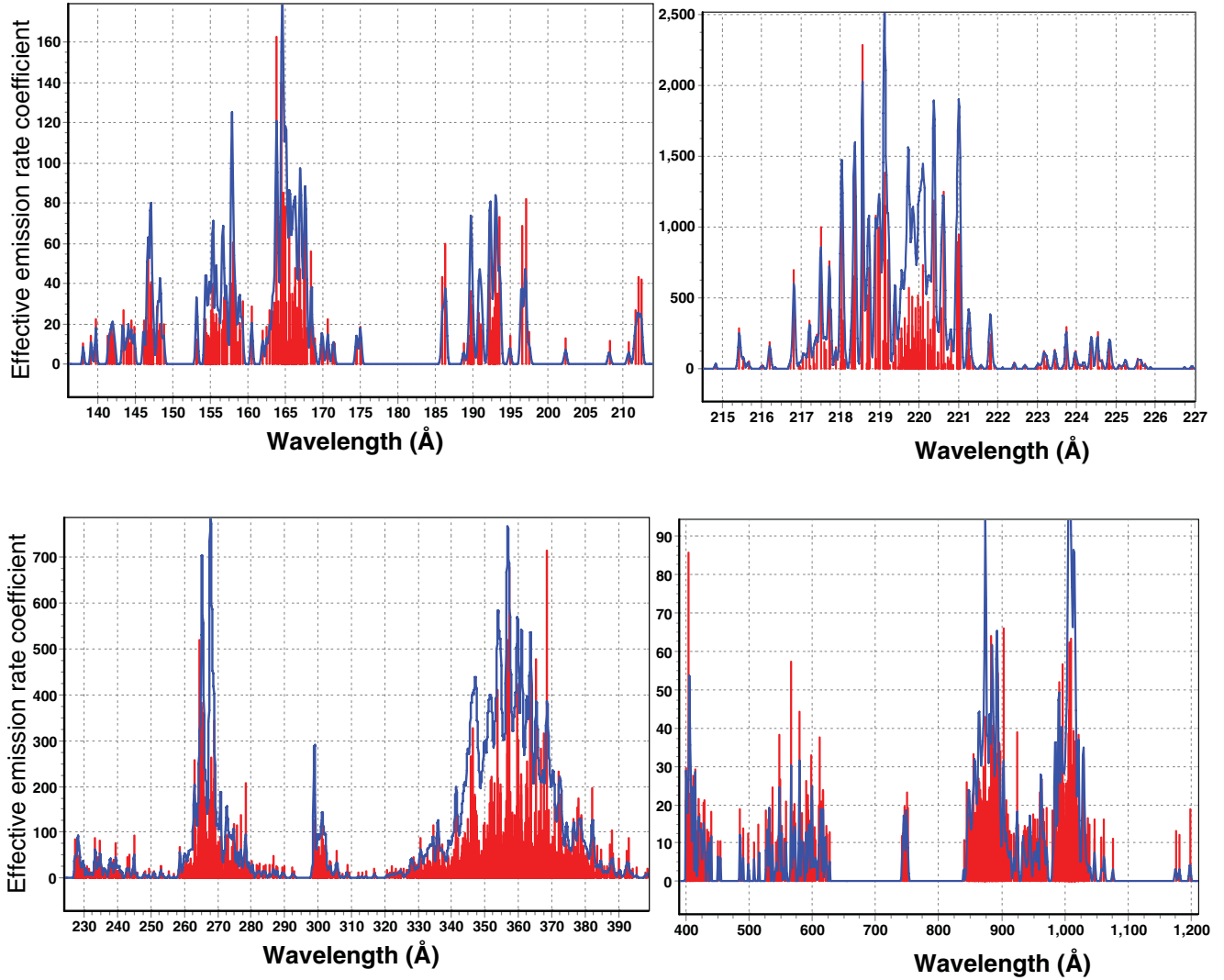
FIG. 1. (Color online) Synthetic spectra of dielectronic satellite lines for transitions between the $4f^{14}5p^55l'nl + 4f^{14}5p^56l''nl + 4f^{13}5p^65l'nl + 4f^{13}5p^66l''nl$ ($l' = d, f$, $l'' = s, p, d, f$, $n = 5$–7) autoionizing states and the $4f^{14}5p^6nl$ single-excited states of Tm-like tungsten at $T_e = 20$ eV. Resolution power, $R = \lambda/\Delta\lambda = 500$ (top left and bottom left panels), 3000 (top right panel), and 400 (bottom right panel), is assumed to produce a Gaussian profile. The scale in the ordinate is in units of 10^{-15} cm^3/s.

the smallest value of temperature at $T_e = 1.38$ eV (curve 1 at the top right panel) and $T_e = 0.46$ eV (curve 1 at the bottom left panel). Other curves (curves 2, 3, and 4) shown at the top right panel of Fig. 3 have maxima at $T_e = 14.6$ eV, 24.7 eV, and 32.1 eV, respectively. Curves 2–5 shown at the bottom left panel of Fig. 3 have two maxima: small maximum around 0.5 eV and higher maximum around 14.6–24.7 eV.

Sum of the contributions from the doubly-excited nonautoionizing $4f^{14}5p^56s^2$, $4f^{14}5p^55d^2$, $4f^{13}5p^66s^2$, $4f^{13}5p^55d^2$, $4f^{14}5p^55d6s$, and $4f^{14}5p^55d6p$ states is illustrated at the bottom right panel of Fig. 3. To obtain $\alpha_d(4f^{14}5p^6, j)$ for the six curves shown in this figure, we sum the $\alpha_d(4f^{14}5p^6, j)$ evaluated for every level included in those configurations. For example, there are 45 and 81 nonautoionizing levels included in the $4f^{14}5p^55d^2$ and $4f^{13}5p^65d^2$ configurations, respectively. The curves 2 and 4 (bottom right panel of Fig. 3) illustrate the values of $\alpha_d(4f^{14}5p^6, j)$ summed over 45 levels for $j = 4f^{14}5p^55d^2$ and summed over 81 levels for $j = 4f^{13}5p^65d^2$.

V. TOTAL DIELECTRONIC RECOMBINATION RATE COEFFICIENT OF Er-LIKE TUNGSTEN

The total DR rate coefficients are obtained by summing the effective emission rate coefficients $C_S^{\text{eff}}(j, i)$ given by Eq. (2) over all possible intermediate and final singly- and doubly-excited states:

$$\alpha_d(i_0) = \sum_i \sum_j C_S^{\text{eff}}(j, i). \qquad (10)$$

We have already discussed the contribution of doubly-excited states with high-n levels [sum over i in Eq. (10)] to the DR rate coefficients. For the total DR rate coefficient, one has to consider the contributions from singly-excited states and nonautoionizing doubly-excited states [sum over j in Eq. (10)]. There are about 340 nonautoionizing doubly excited states in the case of Tm-like tungsten. To illustrate the contribution of the $4f^{13}5p^6n'l'nl(L_{12}S_{12})$ LSJ and $4f^{14}5p^5n'l'nl(L_{12}S_{12})$ LSJ nonautoionizing states to the
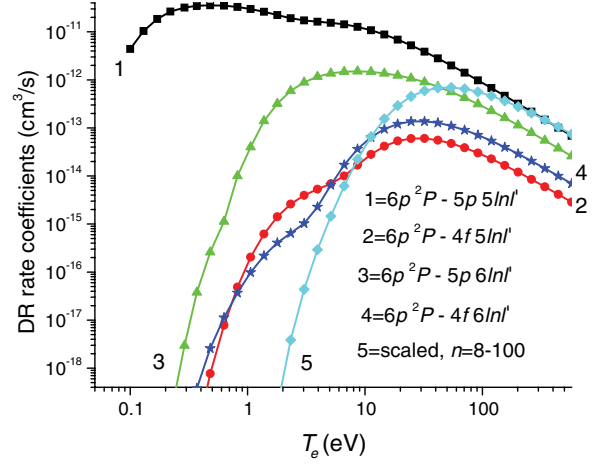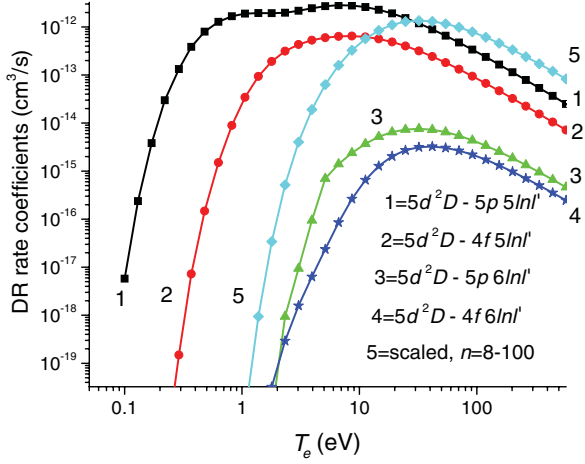
FIG. 2. (Color online) Contributions of the $4f^{14}5p^55l'nl$ ($n = 5$–7), $4f^{13}5p^65l'nl$ ($n = 5$–7), $4f^{14}5p^56l'nl$ ($n = 6$–7), and $4f^{13}5p^66l'nl$ ($n = 6$–7) configurations to the DR rate coefficients $\alpha_d(4f^{14}5p^6, j)$ for $j = 4f^{14}5p^6nl\ ^2L$ states in Tm-like tungsten as a function of T_e. Curve 5 represents the data calculated using scaling formula for n from 8 to 100 (see text for more details).

total DR rate coefficient, we sum those contributions over all angular momenta (L_{12}, S_{12}, L, S, J). Finally, we find $\alpha_d(4f^{14}5p^6, j)$ with $j = [4f^{13}5p^6n'l'nl + 4f^{14}5p^5n'l'nl]$.

The sum of the $\alpha_d(4f^{14}5p^6, j)$ coefficient over j given by doubly-exited, nonautoionizing levels is shown as curve 1 in Fig. 4. In particular, there are five doubly-excited, nonautoionizing $4f^{13}5p^55d^2$, $4f^{13}5p^65d6s$, $4f^{13}5p^65d6p$, and $4f^{14}5p^55d^2$ configurations and three doubly-excited, partially nonautoionizing $4f^{14}5p^56s^2$, $4f^{14}5p^55d6s$, and $4f^{14}5p^55d6p$ configurations. The complete set includes the $4f^{14}5p^55l'nl$ ($l' = f,g$), $4f^{14}5p^56l'nl$, ($l' = p,d,f,g$), $4f^{13}5p^65l'nl$ ($l' = f,g$), and $4f^{13}5p^66l''nl$ ($l' = p,d,f,g$ and $l = s,p,d,f,g$, $n = 6$–7) of the autoionizing configurations.

The contribution from high-n autoionizing levels to the DR rate coefficients involving doubly-excited, nonautoionizing configurations is given by curve 2 of Fig. 4. We follow the procedure described above in Eqs. (5)–(9) for the singly-excited levels to evaluate the scaled values given by curve 2. In the case of the $4f^{14}5p^6nl'$-$4f^{13}5p^6nl'nl$ and $4f^{14}5p^6nl'$-$4f^{14}5p^5nl'nl$ transitions, we use empirical scaling laws, which can only be implemented to include one-electron $4f$-np, $4f$-ng, $5p$-ns, and $5p$-nd transitions. In the case of the $4f^{13}5p^6n_1l_1n_2l_2$-$4f^{13}5p^6n_3l_3n_4l_4$ and $4f^{14}5p^5n_1l_1n_2l_2$-$4f^{14}5p^5n_3l_3n_4l_4$ transitions, we need to consider transitions with $n_1l_1 = n_3l_3$ in the scaling procedure. For example, in the case of the $4f^{13}5p^65d^2$-$4f^{13}5p^6n_3l_3n_4l_4$ transitions, the $4f^{13}5p^65d^2$-$4f^{13}5p^65dnp$ and $4f^{13}5p^6 5d^2$-$4f^{13}5p^65dnf$ transitions need to be included in the scaling procedure. The final result of the scaling procedure given by curve 2 of Fig. 4 shows a maximum at 42 eV. These scaled values given by curve 2 become larger than the main contributions given by curve 1 in the region of large temperature with $T_e > 50$ eV. The ratio of the number of transitions from singly-excited $4f^{14}5p^6nl$ states to autoionizing states to the number of transitions from doubly-excited nonautoionizing states to autoionizing states is very small, only about 12%.

The sum of the contributions from the singly-excited $4f^{14}5p^6nl$ states in Tm-like tungsten to the total DR rate coefficients $\alpha_d(4f^{14}5p^6)$ of Er-like tungsten as a

function of T_e is shown in Fig. 5. Curve 1 displays the $\alpha_d^{\text{sing}}(4f^{14}5p^6) = \sum_i \sum_j C_S^{\text{eff}}(j,i)$ coefficient for $j = 4f^{14}5p^64nl$ ($n = 5$–7) and $i = 4f^{14}5p^55l'nl$ ($n = 5$–7), $4f^{14}5p^56l'nl$ ($n = 6$–7), $4f^{13}5p^65l'nl$ ($n = 5$–7), and $4f^{13}5p^66l''nl$ ($n = 6$–7). Curve 2 displays the $\alpha_d^{\text{sing-scl}}(4f^{14}5p^6) = \sum_i \sum_j C_S^{\text{eff}}(j,i)$ coefficient for $j = 4f^{14}5p^6nl$ ($n = 5$–7) and $i = 4f^{14}5p^55l'nl$, $4f^{14}5p^56l'nl$, $4f^{13}5p^65l'nl$, and $4f^{13}5p^66l''nl$ ($n = 8$–100). The details of the scaling procedure were described by Eqs. (5)–(9).

Curve 3 depicts the contributions from singly-excited levels with high n, i.e., the $4f^{14}5p^6nl$ levels with $n > 7$. For these levels, the $4f^{14}5p^6nl$-$4f^{14}5p^55l'nl$, $4f^{14}5p^6nl$-$4f^{14}5p^56l'nl$, $4f^{14}5p^6nl$-$4f^{13}5p^65l'nl$, and $4f^{14}5p^6nl$-$4f^{13}5p^66l'nl$ transitions are the most important.

To estimate $Q_d(j,i)$ in Eq. (3) with $j = 4f^{14}5p^6nl$ and $i = 4f^{14}5p^5n'l'nl$ and $4f^{13}5p^6n'l'nl$ with $n > 7$, we used the data calculated for $n = 7$ and applied the $1/n^3$ scaling law for the autoionization probabilities A_a and energies E_S. However, the values of A_r for the $4f^{14}5p^6nl$-$4f^{14}5p^5n'l'nl$ and $4f^{14}5p^6nl$-$4f^{13}5p^6n'l'nl$ transitions are almost independent of n since they are, in fact, one-electron transitions where the nl electron is a spectator (see, for example, Ref. [31]). The final values of the $\alpha_d^{\text{sing-sc2}}(4f^{14}5p^6) = \sum_i \sum_j C_S^{\text{eff}}(j,i)$ term for $j = 4f^{14}5p^6nl$ ($n = 8$–500) and $i = 4f^{14}5p^55l'nl$, $4f^{14}5p^56l'nl$, $4f^{13}5p^65l'nl$, and $4f^{13}5p^66l'nl$ ($n = 8$–500) are plotted by curve 3 of Fig. 5. We increased the number of states in sum over n ($n = 500$ instead of $n = 100$) in comparison with the number of states in sum over n used to describe curve 2 in Fig. 5. Those changes are due to slower convergence.

The $\alpha_d^{\text{sing-sc2}}(4f^{14}5p^6)$ values are larger than the $\alpha_d^{\text{sing-scl}}(4f^{14}5p^6)$ values by a factor of 10. The maximum values of the curves 2 and 3 are near 42 and 25 eV, respectively. Curve 1 has a maximum for a very small temperature, i.e., about 1 eV.

In Fig. 6, we illustrate the results for the total DR rate coefficient $\alpha_d(4f^{14}5p^6)$ in Er-like tungsten. The electron
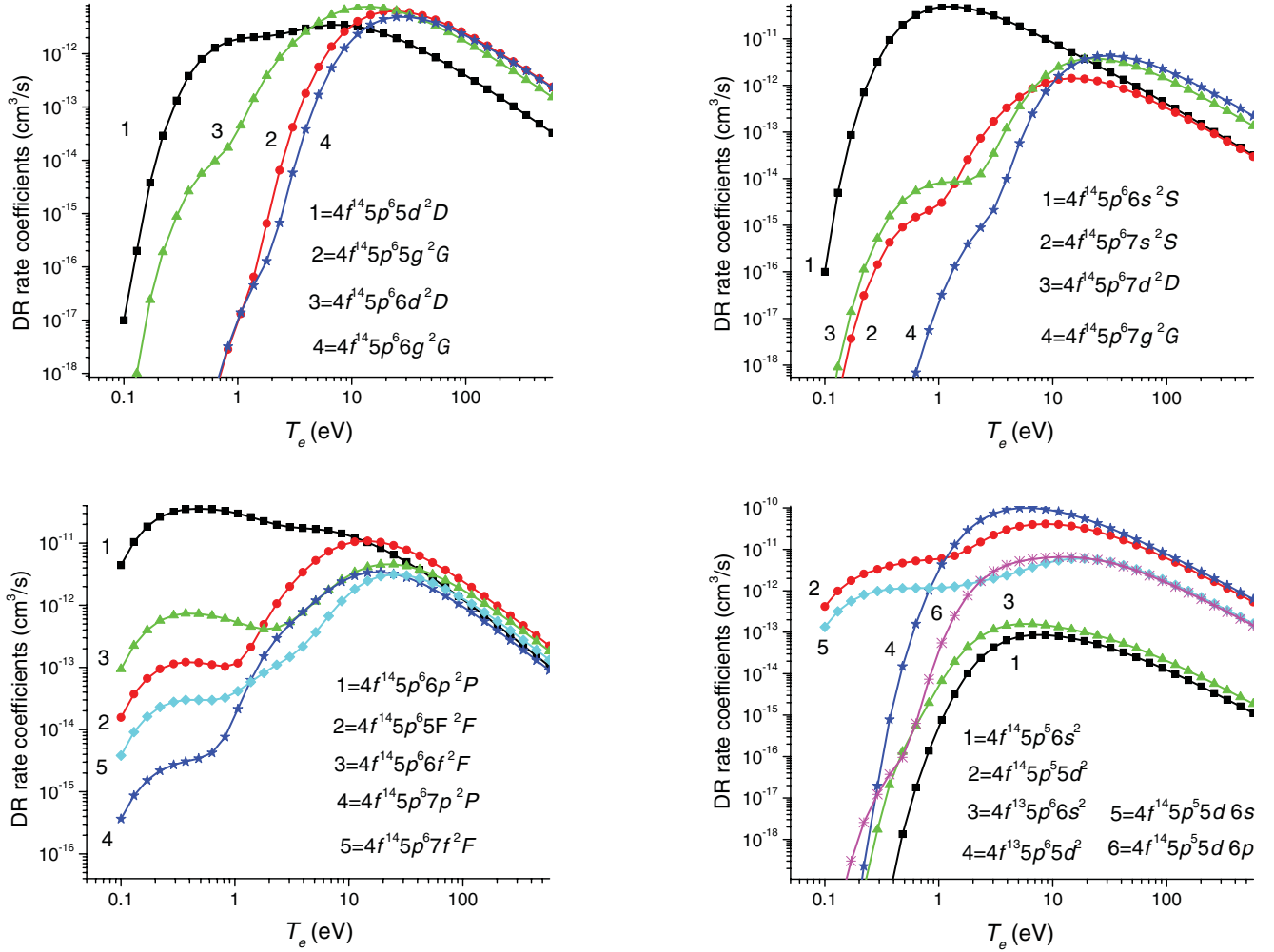
FIG. 3. (Color online) DR rate coefficients $\alpha_d(4f^{14}5p^6, j)$ for the $j = 4f^{14}5p^6ns\ ^2S, 4f^{14}5p^6np\ ^2P, 4f^{14}5p^6nd\ ^2D, 4f^{14}5p^6nf\ ^2F$, and $4f^{14}5p^6ng\ ^2G$ levels in Tm-like tungsten as a function of T_e.

temperature varies between 0.1 and 580 eV. The resulting curve labeled 4 has a maximum at $T_e \approx 25$ eV and very slowly decreases from a maximum value of 7.7×10^{-10} cm^3/s to 7.0×10^{-11} cm^3/s at 340 eV. Different contributions are illustrated by curves 1 through 3. Curve 1 depicts the $\alpha_d^{\text{sing}}(4f^{14}5p^6)$, corresponding to curve 1 of Fig. 5. Curve 2 displays $\alpha_d^{\text{doub}}(4f^{14}5p^6)$ that was illustrated by curve 1 of Fig. 4. Curve 3 shows the combined scaled contributions illustrated by curve 2 of Fig. 4 [$\alpha_d^{\text{doub}}(4f^{14}5p^6)$] and curves 2 and 3 of Fig. 5. It is evident from Fig. 6 that those three contributions $\alpha_d^{\text{sing}}(4f^{14}5p^6)$, $\alpha_d^{\text{doub}}(4f^{14}5p^6)$, and $\alpha_d^{\text{scale}}(4f^{14}5p^6)$ give the largest contributions to the $\alpha_d^{\text{total}}(4f^{14}5p^6)$ in the different ranges of temperature. For the smallest $T_e = 0.1–1$ eV, the dominant contribution comes from [$\alpha_d^{\text{sing}}(4f^{14}5p^6)$] given by curve 1. Curve 2 [$\alpha_d^{\text{doub}}(4f^{14}5p^6)$] has a maximum around 6.65 eV, while curve 3 [$\alpha_d^{\text{scale}}(4f^{14}5p^6)$] has a maximum around 24.7 eV. The scaled contribution becomes a dominant contribution to the total DR coefficient for the high-temperature region starting from 25 eV.

The tabulated values of the total rate coefficient α_d^{total} are presented in Table VIII for $T_e = 0.1$ to 580 eV on a logarithmic grid $T_e = (0.1 \times 1.3^{N-1})$ eV with $N = 1$–34.

VI. UNCERTAINTY ESTIMATES AND CONCLUSION

In the present paper, we calculated a large set of atomic data needed to describe the dielectronic recombination of the Er-like W^{6+} into Tm-like W^{5+}. Energy levels, wavelengths, weighted radiative transition probabilities, and autoionization rates are calculated for the Tm-like tungsten ion using two theoretical methods, namely, the Hartree-Fock-relativistic method (COWAN code) and the relativistic many-body perturbation theory method (RMBPT code) for a limited number of states. In order to check the accuracy of those calculations, we performed additional calculations using the second- and third-order relativistic perturbation theory and relativistic SD all-order method. The SD method, which is a linearized coupled-cluster method, includes correlation corrections in a more complete way and is expected to yield more accurate results, especially when correlation corrections are significant. While the SD method includes fourth- and higher-order terms, it omits some third-order terms. These omitted terms are identified and added to our SD data. Also, comparison is made with all available NIST data.

The largest disagreement (0.2%) between our $E^{(\text{DF+SD})}$ and $E^{(\text{NIST})}$ values occurs for the $5f\ ^2F_J$ levels. We find
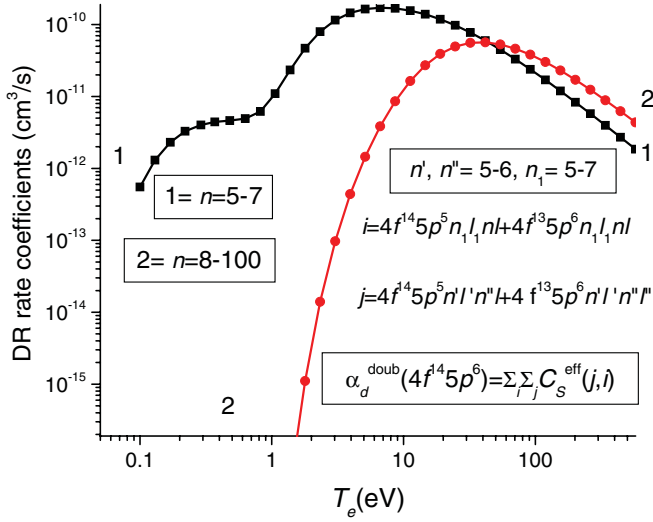
FIG. 4. (Color online) Sum of the contributions from the doubly-excited nonautoionizing $4f^{14}5p^56s^2$, $4f^{14}5p^55d^2$, $4f^{14}5p^55d6s$, $4f^{14}5p^55d6p$, $4f^{13}5p^66s^2$, $4f^{13}5p^55d^2$, $4f^{13}5p^65d6s$, and $4f^{13}5p^65d6p$ configurations of Tm-like tungsten to the total DR rate coefficients $\alpha_d(4f^{14}5p^6)$ of Er-like tungsten as function of T_e.

an excellent agreement (0.01%) between our $E^{(DF+SD)}$ and $E^{(NIST)}$ values for ionization potential [19], which is well within the experimental uncertainty of 0.06%. The energies calculated by COWAN code are in a good agreement with the second-order RMBPT energies ($E^{(DF+2)}$), because the large portion of correlation contribution is taken into account by atomic structure code of COWAN [32] with scaling of the electrostatic integrals. The accuracy of oscillator strengths and transition rates is estimated to be about 20%–50% for the largest gf and gA_r values and a factor of 2–5 for the smallest ones. Such large differences are due to substantial contribution of correlation effects. The accuracy of autoionizing rates gA_a are about 20%–40% for the largest values of gA_a ($gAa \simeq 10^{13}$–10^{14} s^{-1}).
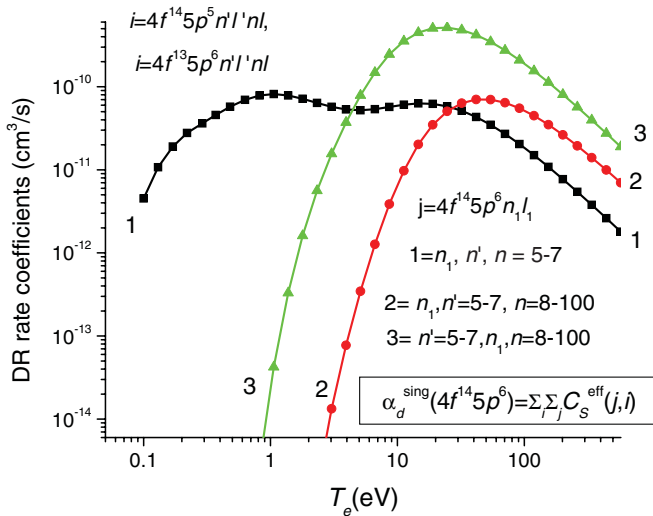

FIG. 5. (Color online) Sum of the contributions from the singly-excited $4f^{14}5p^6nl$ states of Tm-like tungsten to the total DR rate coefficients $\alpha_d(4f^{14}5p^6)$ of Er-like tungsten as function of T_e.
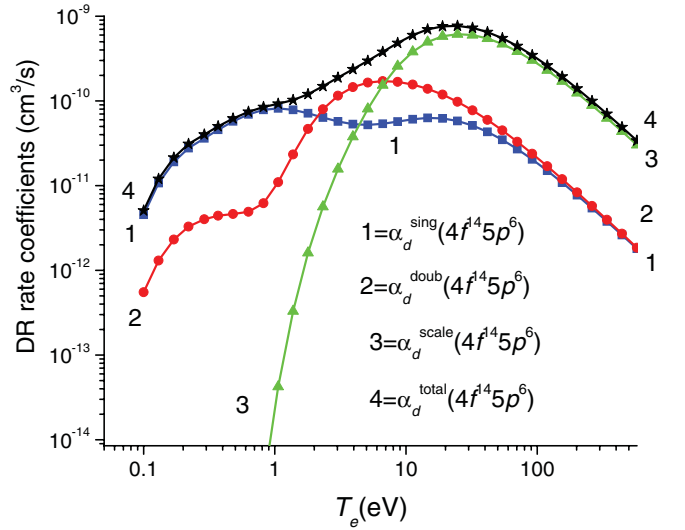

FIG. 6. (Color online) Contributions from the singly-excited $\alpha_d^{sing}(4f^{14}5p^6)$ and doubly-excited nonautoionizing $\alpha_d^{doub}(4f^{14}5p^6)$ states to the total DR rate coefficients $\alpha_d(4f^{14}5p^6)$ in Er-like tungsten as function of T_e. Curve 3 shows the combined scaled contributions illustrated by curve 2 of Fig. 4 and curves 2 and 3 of Fig. 5.

The calculated atomic data are used to obtain the dielectronic satellite lines as well as the DR rate coefficients. The doubly-excited $4f^{14}5p^55l'nl$ ($n = 5$–7), $4f^{14}5p^56l'nl$ ($n = 6$–7), $4f^{13}5p^65l'nl$ ($n = 5$–7), and $4f^{13}5p^66l''nl$ ($n = 6$–7) configurations are taken into account to calculate the DR rate coefficients. We find that the contributions of the highly-excited states are very important for the calculation of total DR rates. We estimated these contributions using the approximate formulas for n up to 100. We calculated the state-selective DR rate coefficients from the ground state of Er-like W ion to the Tm-like W ion for the singly-excited $4f^{14}5p^6nl$ ($n = 5$–7), as well as eight doubly-excited, nonautoionizing $4f^{13}5p^55d^2$, $4f^{13}5p^65d6s$, $4f^{13}5p^65d6p$,

TABLE VIII. Total DR rate coefficients of Er-like tungsten (in cm^3/s) α_d^{total} as a function of T_e (in eV). $A[B]$ means $A \times 10^B$.

T_e (eV)	α_d^{total}	T_e (eV)	α_d^{total}
0.10	5.08[−12]	8.65	4.82[−10]
0.13	1.20[−11]	11.25	5.97[−10]
0.17	2.14[−11]	14.62	6.98[−10]
0.22	3.11[−11]	19.00	7.60[−10]
0.29	4.02[−11]	24.71	7.70[−10]
0.37	5.01[−11]	32.12	7.29[−10]
0.48	6.20[−11]	41.75	6.50[−10]
0.63	7.44[−11]	54.28	5.50[−10]
0.82	8.47[−11]	70.56	4.45[−10]
1.06	9.26[−11]	91.73	3.47[−10]
1.38	1.02[−10]	119.25	2.62[−10]
1.79	1.20[−10]	155.03	1.94[−10]
2.33	1.49[−10]	201.54	1.40[−10]
3.03	1.88[−10]	262.00	9.98[−11]
3.94	2.37[−10]	340.60	7.03[−11]
5.12	2.97[−10]	442.78	4.90[−11]
6.65	3.78[−10]	575.61	3.39[−11]

$4f^{14}5p^55d^2$, $4f^{14}5p^56s^2$, $4f^{14}5p^55d6s$, and $4f^{14}5p^55d6p$ configurations. Contributions from the doubly-excited nonautoionizing states are found to be very important in the determination of the total DR coefficient.

The accuracy of transition radiative and nonradiative rates, and wavelengths, given in columns "A_a,""gA_r,"and "λ"of Tables IV–VII was discussed in Sec. II. The intensity factor Q_d [Eq. (3)] includes a product $gA_a \times A_r$ and the sum of A_a and A_r. Comparing results given in columns "A_a"and "$\sum gA_r$,"we find that $A_a \gg A_r$. Then, Q_d can be estimated as $Q_d(j,i) \approx g(i)A_r(j,i)$. The accuracy of radiative transition rates A_r was estimated in previous sections as 20%–50% for the largest A_r values and a factor of 2–5 for the smallest one. Therefore, the accuracy of Q_d values should be 20%–50%, since we list the largest Q_d values in Tables IV–VII. The accuracy of the effective emission rate coefficient $C_S^{\text{eff}} \approx Q_d\exp[-E_s(i)/kT_e]$ (see the last column of Tables IV–VII) depends on the accuracy of the Q_d and the excitation energies E_S. The E_S values (see the fourth column of Tables IV–VII) are defined as the excitation energy (called Auger energies) of the autoionizing state relative to the energy of the $4f^{14}5p^6$ threshold. We use NIST value for the threshold, which has 0.06% uncertainty (522370 ± 300) [19]. We believe that the accuracy of autoionizing state energies is similar to the accuracy of nonautoionizing states given in Table II. The estimate of the wavelength accuracy for doubly-excited states in W^{27+} ion was carried out in Ref. [40]. The accuracy was estimated to be about 0.3%–0.6% for most of the transitions. The theoretical accuracy of energy values decreases for low-ionized tungsten. In recent work [41], wavelengths for the dipole transitions in Er-like W^{6+} ion calculated using RMBPT, COWAN, and HULLAC codes were compared with recommended NIST data [19]. We found the estimate of wavelengths calculated by COWAN code to be accurate to 2%–3%. Therefore, we can conclude that the effective emission rate coefficients C_S^{eff} are accurate to 25%–55% for most of the cases given in Tables IV–VII.

The total rate coefficient is defined as a sum over i and j indexes of the effective emission rate coefficients $C_S^{\text{eff}}(i,j)$ [see Eq. (10)]. We estimated the accuracy of the effective emission rate coefficients C_S^{eff} to be 25%–55%. This estimate holds for the part of sum over i and j indexes in Eq. (10) up to $i = 7$ and $j = 7$. We use scaled values for the sum in Eq. (10) for $i = 8$–100 and $j = 8$–100. The contribution of scaled values in α_d^{total} is not important for small temperature $T_e = 0.1$–2 eV. This contribution increases with increasing T_e: 0.5% for $T_e = 2.3$ eV, 52% for $T_e = 8.6$ eV, and 86% for $T_e = 71$ eV. Therefore, we can conclude that the accuracy of α_d^{total} is about 25%–55% for small temperatures and about a factor of 2 for $T_e > 8$ eV.

[1] S. Schippers, D. Bernhardt, A. Müller, C. Krantz, M. Grieser, R. Repnow, A. Wolf, M. Lestinsky, M. Hahn, O. Novotný *et al.*, Phys. Rev. A **83**, 012711 (2011).

[2] U. I. Safronova, A. S. Safronova, P. Beiersdorfer, and W. R. Johnson, J. Phys. B **44**, 035005 (2011).

[3] U. I. Safronova, A. S. Safronova, and P. Beiersdorfer, Can. J. Phys. **89**, 581 (2011).

[4] U. I. Safronova, A. S. Safronova, and W. R. Johnson, J. Phys. B **43**, 144001 (2010).

[5] U. I. Safronova, A. S. Safronova, and P. Beiersdorfer, At. Data Nucl. Data Tables **95**, 751 (2009).

[6] U. I. Safronova, A. S. Safronova, and P. Beiersdorfer, J. Phys. B **42**, 165010 (2009).

[7] C. Biedermann and R. Radtke, AIP Conf. Proc. **1161**, 95 (2009).

[8] C. Biedermann, R. Radtke, R. Seidel, and E. Behar, J. Phys. Conf. Series **163**, 012034 (2009).

[9] F.-C.Meng, L. Zhou, M.Huang, C.-Y. Chen, Y.-S. Wang, and Y.-M. Zou, J. Phys. B **42**, 105203 (2009).

[10] F.-C. Meng, C.-Y. Chen, Y.-S. Wang, and Y.-M. Zou, J. Quant. Spectrosc. Radiat. Transf. **109**, 2000 (2008).

[11] C. P. Ballance, S. D. Loch, M. S. Pindzola, and D. C. Griffin, J. Phys. B **43**, 205201 (2010).

[12] S. Dalhed, J. Nilsen, and P. Hagelstein, Phys. Rev. A **33**, 264 (1986).

[13] E. Behar, A. Peleg, R. Doron, P. Mandelbaum, and J. L. Schwob, J. Quant. Spectrosc. Radiat. Transf. **58**, 449 (1997).

[14] E. Behar, R. Doron, P. Mandelbaum, and J. L. Schwob, Phys. Rev. A **58**, 2115 (1998).

[15] E. Behar, P. Mandelbaum, and J. L. Schwob, Phys. Rev. A **59**, 2787 (1999).

[16] E. Behar, R. Doron, P. Mandelbaum, and J. L. Schwob, Phys. Rev. A **61**, 062708 (2000).

[17] A. Peleg, E. Behar, P. Mandelbaum, and J. L. Schwob, Phys. Rev. A **57**, 3493 (1998).

[18] E. Behar, P. Mandelbaum, and J. L. Schwob, Eur. Phys. J. D **7**, 157 (1999).

[19] A. E. Kramida and T. Shirai, At. Data Nucl. Data Tables **95**, 305 (2009).

[20] U. I. Safronova and T. Kato, J. Phys. B **31**, 2501 (1998).

[21] U. I. Safronova and T. Kato, Phys. Scr. **53**, 461 (1996).

[22] T. Kato, U. I. Safronova, and M. Ohira, Phys. Scr. **55**, 185 (1997).

[23] U. I. Safronova, T. Kato, and M. Ohira, J. Quant. Spectrosc. Radiat. Transfer **58**, 193 (1997).

[24] I. Murakami, U. I. Safronova, A. A. Vasilyev, and T. Kato, At. Data Nucl. Data Tables **90**, 1 (2005).

[25] I. Murakami, U. I. Safronova, and T. Kato, Can. J. Phys. **80**, 1525 (2002).

[26] I. Murakami, U. I. Safronova, and T. Kato, J. Phys. B **32**, 5351 (1999).

[27] U. I. Safronova and R. Mancini, At. Data Nucl. Data Tables **95**, 54 (2009).

[28] I. Murakami, T. Kato, D.Kato, U. I. Safronova, T. E. Cowan, and Yu. Ralchenko, J. Phys. B **39**, 1 (2006).

[29] I. Murakami, U. I. Safronova, and T. Kato, J. Phys. Conf. Series **163**, 012061 (2009).

[30] U. I. Safronova, P. Wilcox, and A. S. Safronova, J. Phys. B **44**, 225002 (2011).

[31] U. I. Safronova, R. Bista, R. Bruch, and Yu. Ralchenko, J. Phys. B **42**, 015001 (2009).

[32] R. D. Cowan, *The Theory of Atomic Structure and Spectra* (University of California Press, Berkeley, 1981).

[33] URL [http://das101.isan.troitsk.ru/cowan.htm].

[34] W. R. Johnson, Z. W. Liu, and J. Sapirstein, At. Data Nucl. Data Tables **64**, 279 (1996).

[35] S. A. Blundell, W. R. Johnson, and J. Sapirstein, Phys. Rev. A **43**, 3407 (1991).

[36] M. S. Safronova, W. R. Johnson, and A. Derevianko, Phys. Rev. A **60**, 4476 (1999).

[37] W. R. Johnson, S. A. Blundell, and J. Sapirstein, Phys. Rev. A **37**, 307 (1988).

[38] J. Dubau and S. Volonte, Rep. Prog. Phys. **43**, 199 (1980).

[39] U. I. Safronova, I. Y. Tolstikhina, R. Bruch, T. Tanaka, F. Hao, and D. Schneider, Phys. Scr. **47**, 364 (1993).

[40] U. I. Safronova and A. S. Safronova, Can. J. Phys. **87**, 83 (2009).

[41] U. I. Safronova and A. S. Safronova, Phys. Rev. A **84**, 012511 (2011).